



NLR-TP-2014-096

## **Numerical simulations for high offset intake diffuser flows**

T.M. Berens, A.-L. Delot, M. Chevalier and J. van Muijden

**Nationaal Lucht- en Ruimtevaartlaboratorium**

National Aerospace Laboratory NLR

Anthony Fokkerweg 2

P.O. Box 90502

1006 BM Amsterdam

The Netherlands

Telephone +31 (0)88 511 31 13

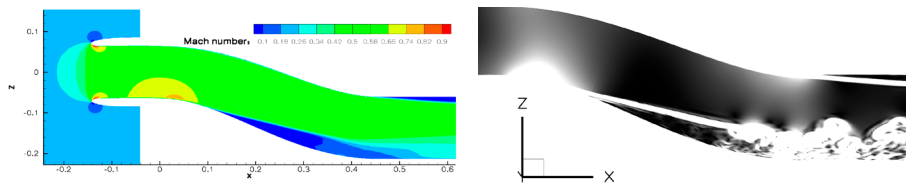
Fax +31 (0)88 511 32 10

[www.nlr.nl](http://www.nlr.nl)



## Executive summary

# Numerical simulations for high offset intake diffuser flows



### Report no.

NLR-TP-2014-096

### Author(s)

T.M. Berens  
A.-L. Delot  
M. Chevalier  
J. van Muijden

### Report classification

UNCLASSIFIED

### Date

February 2014

### Knowledge area(s)

Computational Physics en  
theoretische aërodynamica

### Descriptor(s)

intake diffuser  
high offset  
low-observability  
propulsion integration  
aerodynamic performance

### Problem area

The design of intake diffusers for fighter aircraft and unmanned aerial vehicles usually exhibits a high degree of offset between intake and engine face and tends towards compactness. The design driver for these choices is mainly based on low observability in terms of radar cross section area, and on weight requirements. The resulting non-optimal aerodynamic characteristics of the S-shaped intake duct have to be accepted even though it may lead to adversely affected engine performance. For the analysis of the aerodynamic characteristics of such an intake duct and its consequences on engine performance, it is of utmost importance to be able to accurately assess the flow phenomena at hand.

CFD-analysis of the flow, based on the Reynolds-averaged Navier-Stokes (RANS) equations, is in general not capable of meeting the challenges of these internal flow

fields. Thus, the application of hybrid RANS-Large Eddy Simulation (LES) is investigated in terms of predictive potential for these difficult internal flows. Research on the application of hybrid RANS-LES has been executed in the framework of the aerodynamics action group (AD) AG-43 entitled “Application of CFD to high offset intake diffusers” of the Group for Aeronautical Research and Technology in Europe (GARTEUR). In this group, five international partners cooperated on the investigation of flow predictions for an S-shaped intake duct, not only using RANS methods but also a variety of hybrid RANS-LES simulation methods. This group was active in the period 2005 to 2011, and the final GARTEUR report from the action group was publicly released in October 2012. The current report is a summary of the results from the hybrid RANS-LES simulations of different partners.

**Description of work**

The RAE M2129 S-shaped intake duct was selected as test case for the GARTEUR (AD) AG-43 action group. The geometrical description of the intake channel, experimental test data and initial common meshes were provided for the study. Hybrid RANS-LES simulation results have been compared with steady and unsteady RANS simulations obtained by several partners, as well as with experimental results from wind tunnel tests. Specific distortion parameters (denoted as DC60) based on total pressure data have been derived from the flow field and compared with experiment. For some partners, the initial common meshes proved to be too restrictive and even finer meshes were generated to allow for mesh refinement studies and enhanced resolution in the flow fields.

**Results and conclusions**

It is found that data derived from hybrid RANS-LES simulations in general are in accordance with experimental values, but in the future accuracy levels will need to be improved to enhance reliability for predictions as required by industrial standards. Recorded total pressure fluctuations for different sensor points in the flow field very well demonstrated the highly turbulent character of the flow in the separated region downstream of

the S-bend in the diffuser and require further analysis with respect to resonance frequencies that could be harmful to compressor blades. The evaluation of the distortion parameter DC60 based on total pressures of the intake flow at the engine face revealed that only dynamic simulations can lead to a correct assessment of the performance parameters reflecting the distortion limits required by the engine manufacturers. The grid resolution and physical time step size turned out to be important constraints impacting the computational results and hence the instantaneous distortion parameters.

**Applicability**

Hybrid RANS-LES results for the GARTEUR (AD) AG-43 action group were obtained several years ago. Since then, developments have continued. At NLR, improved flow solver settings and higher-order capabilities have been devised to allow for higher accuracy and significantly less artificial dissipation, thereby improving the realism in the initiation and development of unsteadiness in flow fields. In view of the rapidly progressing developments in hybrid RANS-LES methods, the current status of predictive performance is believed to be readily applicable to complex flows involving large areas of flow separation, and will be evolving in the forthcoming years.



NLR-TP-2014-096

## Numerical simulations for high offset intake diffuser flows

T.M. Berens<sup>1</sup>, A.-L. Delot<sup>2</sup>, M. Chevalier<sup>3</sup> and J. van Muijden

<sup>1</sup> CASSIDIAN EADS Deutschland GmbH

<sup>2</sup> ONERA

<sup>3</sup> FOI

This report is based on a presentation held at the 52<sup>nd</sup> AIAA Aerospace Sciences Meeting, National Harbor, Maryland, 13-17 January 2014.

The contents of this report may be cited on condition that full credit is given to NLR and the authors.  
This publication has been refereed by the Advisory Committee AEROSPACE VEHICLES.

Customer                      National Aerospace Laboratory NLR  
Contract number            -----  
Owner                         NLR  
Division NLR                 Aerospace Vehicles  
Distribution                 Unlimited  
Classification of title      Unclassified  
   February 2014

Approved by:

Author J. van Muijden 	Reviewer B.B. Prananta 	Managing department K.M.J. de Cock 
Date: 28-02-2014	Date: 28/02/2014	Date: 3/3/2014



## Contents

<b>Nomenclature</b>	<b>6</b>
<b>1 Introduction</b>	<b>7</b>
<b>2 Test Case and Experimental Data</b>	<b>8</b>
2.1 RAE M2129 S-Diffuser Geometry	8
2.2 Experimental Data for Comparison with Numerical Results	8
<b>3 Grid Generation, Boundary Conditions, and Numerical Methods Applied</b>	<b>9</b>
3.1 Grid Generation	9
3.2 Boundary Conditions	10
3.3 Numerical Methods Applied by FOI	10
3.4 Numerical Methods Applied by ONERA	11
3.5 Numerical Methods Applied by NLR	12
3.6 Numerical Methods Applied by EADS Cassidian	13
<b>4 Numerical Results</b>	<b>14</b>
4.1 Numerical Results of RANS and URANS Computations	14
4.2 Numerical Results of DES Simulations	18
<b>5 Conclusion</b>	<b>30</b>
<b>Acknowledgments</b>	<b>31</b>
<b>References</b>	<b>31</b>



This page is intentionally left blank.

# Numerical Simulations for High Offset Intake Diffuser Flows

A. Thomas M. Berens<sup>1</sup>

*CASSIDIAN EADS Deutschland GmbH, 85077 Manching, Germany*

B. Anne-Laure Delot<sup>2</sup>

*ONERA – The French Aerospace Lab, F-92190 Meudon, France*

C. Mattias Chevalier<sup>3</sup>

*Swedish Defence Research Agency (FOI), SE-16490 Stockholm, Sweden*

*and*

D. Jaap van Muijden<sup>4</sup>

*National Aerospace Laboratory - NLR, 1059 CM Amsterdam, The Netherlands*

The design of intake diffusers for application in unmanned aerial vehicles tends towards compactness and a high degree of offset between intake and engine face due mainly to low-observability and weight requirements. This leads to non-optimal aerodynamics, generating flow characteristics which can adversely affect engine performance. Thus, the ability to accurately predict the aerodynamics of highly offset diffuser shapes and their performance is of great significance for intake design and aerodynamic propulsion integration. For this type of flow, Computational Fluid Dynamics (CFD) prediction capabilities based on a Reynolds-Averaged-Navier-Stokes (RANS) model approach do not meet the challenges these internal flow fields imply. In contrast, Detached Eddy Simulation (DES) as an advanced hybrid method offers the potential to provide accurate predictions at an acceptable computational cost. Within the Aerodynamics Action Group AD/AG-43 "Application of CFD to High Offset Intake Diffusers" of the Group for Aeronautical Research and Technology in Europe (GARTEUR), DES simulations were performed for the Royal Aircraft Establishment (RAE, a predecessor of QinetiQ) M2129 S-shaped diffuser. Numerical results were compared with steady RANS and unsteady RANS (URANS) data as well as with experimental results from tests conducted for this configuration at RAE Bedford (UK) in the 13ft x 9ft wind tunnel. DES data in general were in accordance with the experimental values, but in the future accuracy levels will need to be improved to enhance reliability for predictions required by industrial standards. Recorded total pressure fluctuations for different sensor points in the flow field very well demonstrated the highly turbulent character of the flow in the separated region downstream of the S-bend in the diffuser and require further analysis with respect to resonance frequencies, which might be harmful to compressor blades. The evaluation of the distortion parameter DC60 based on total pressures generated by steady state (e.g. RANS) and dynamic simulation methods of the intake flow at the engine face revealed that only dynamic simulations can lead to a correct assessment of the performance parameters reflecting the distortion limits required by the engine manufacturers. The grid resolution and the physical time step size turned out to be important constraints impacting the computational results and hence the instantaneous distortion parameters.

---

<sup>1</sup> Expert Aerodynamic Propulsion Integration and Internal Aerodynamics, Flight Physics/Aerodynamics & Methods, Rechliner Strasse/COEAI1, Associate Fellow AIAA.

<sup>2</sup> Research Scientist, Applied Aerodynamics Department, 8 Rue des Vertugadins, Senior Member AIAA.

<sup>3</sup> Senior Scientist, Computational Physics, Gullfossгатan 6.

<sup>4</sup> Senior Scientist, Flight Physics and Loads Department, Anthony Fokkerweg 2, Senior Member AIAA.

## Nomenclature

$Alt$	=	altitude
$A_c$	=	intake capture area
$A_0$	=	cross section of captured stream tube at infinity
$A_0/A_c$	=	mass flow ratio (MFR), area ratio of captured stream tube
$DC60$	=	circumferential distortion coefficient
$H, p_t$	=	total pressure
$H_{ef}$	=	area-weighted average total pressure at the engine face
$HRA (H_{ef}/H_\infty), hr$	=	total pressure recovery (EtaTotalPressure $p_t/p_{t\infty}$ )
$H_\infty, H_0, p_{t\infty}$	=	total pressure at infinity
$H_{60 min}$	=	mean total pressure in the worst 60 deg sector of the engine face
$M, Ma, m, mach$	=	Mach number
$mean$	=	time-averaged
$p$	=	pressure
$P$	=	total pressure
$pr, PRA, pra$	=	time-averaged static pressure/total pressure at infinity
$MF (MFR)$	=	mass flow (mass flow ratio)
$Q$	=	dynamic pressure
$qr$	=	time-averaged dynamic pressure/total pressure at infinity
$Re$	=	Reynolds number
$T, Temp$	=	static temperature
$T$	=	time period
$t, tot$	=	total state
$T_t$	=	total temperature
$v$	=	velocity
$x, y, z$	=	coordinates in reference coordinate system
$\alpha$	=	angle of attack
$\beta$	=	angle of sideslip
$\eta$	=	total pressure recovery
$\Delta t$	=	time step size
$\rho$	=	density
$\infty, inf, 0$	=	ambient condition, state at infinity, free stream condition

AG	Action Group
AD	Aerodynamics
AIP	Aerodynamic Interface Plane
CEP, ef	Compressor Entry Plane, engine face
CFD	Computational Fluid Dynamics
DDES	Delayed Detached Eddy Simulation
DES	Detached Eddy Simulation
DNS	Direct Numerical Simulation
exp	experimental value
GARTEUR	Group for Aeronautical Research and Technology in EUROpe
LES	Large Eddy Simulation
RAE	Royal Aircraft Establishment
RANS	Reynolds-Averaged Navier-Stokes
S-A	Spalart-Allmaras (turbulence model)
STBD	Starboard
URANS	Unsteady Reynolds-Averaged Navier-Stokes
X-LES	eXtra-Large Eddy Simulation (method by NLR)
ZDES	Zonal Detached Eddy Simulation

## 1 Introduction

**A**ERODYNAMIC propulsion integration for unmanned aerial vehicles includes the design of compact intake diffusers with a high degree of offset between intake and engine face, due to mainly weight and stealth factors. In order to improve low-observability characteristics of the propulsion system shielding of the engine face from direct observation is mandatory. Due to geometrical constraints of the intake design complex three-dimensional flow characteristics might be generated which can adversely affect intake flow stability and hence engine performance, producing a decrease in thrust and a reduced engine surge margin. As a result, there is a need for a direct compromise to be made between observability and other vehicle attributes such as range or cost. Current diffuser flow management and control systems are largely empirically derived, and cost intensive wind tunnel experiments need to be performed in order to optimize the design. Improved understanding of the flow physics in this class of diffuser could lead to improved methodologies for controlling such flows, resulting in greater low-observability design flexibility and a more favorable signature versus cost trade-off. Thus, for efficient propulsion integration the ability to accurately predict the unsteady aerodynamics of highly offset diffuser shapes and to assess the engine/intake compatibility is of great significance.

Conventional Computational Fluid Dynamics (CFD) prediction capabilities for this type of flow, based on solutions of the Reynolds-Averaged Navier-Stokes (RANS) equations, do not meet the challenges these internal flow fields imply. The extension of the RANS approach to capture the time-evolution of the flow (Unsteady RANS or URANS) leads to the possibility for improved predictions, and further development of this approach is in progress. While the use of Direct Numerical Simulation (DNS) or Large Eddy Simulation (LES) methods could, in principle, deliver predictions of the flow physics to the desired level of accuracy, their general use is still unfeasible, due to the vast amount of computing power required. Detached Eddy Simulation (DES) as an advanced method in CFD offers great potential for simulation and analysis of unsteady aerodynamic flow fields,<sup>1-6</sup> where high turbulence levels and instantaneous phenomena occur, and for the evaluation of their impact on performance parameters. At acceptable computational costs these hybrid RANS-LES turbulence methods offer the chance to combine the physical accuracy of the LES and the cost-effectiveness of the RANS methods.<sup>3,7</sup> The hybrid models, as originally proposed, are designed to treat the entire boundary layer using a RANS model and to apply a LES treatment to separated regions.

The Aerodynamics Action Group AD/AG-43 "Application of CFD to High Offset Intake Diffusers" of the Group for Aeronautical Research and Technology in EUROpe<sup>8</sup> (GARTEUR) was installed to provide a greater insight into the potential of DES for the accurate prediction of flow in serpentine intake diffusers. Within the frame of the numerical investigations in GARTEUR AD/AG-43, which were performed between 2005 and 2011, with EADS CASSIDIAN (Germany), ONERA (France), FOI (Sweden), NLR (The Netherlands) and QinetiQ (United Kingdom) as partners, conventional CFD and DES methods were applied for the simulation of internal flow in the Royal Aircraft Establishment (RAE, a predecessor of QinetiQ) M2129 diffuser with separation and reattachment as involved flow physics. The main objectives were to study the time-dependant behavior of the flow and the impact on the total pressure recovery in the engine face as the basic parameter for the assessment of intake flow distortion and engine/intake compatibility as well as to compare the applied simulation methods. Various turbulence models were applied and the numerical results were compared with a set of experimental data gathered with the RAE M2129 S-diffuser model in wind tunnel tests.

## 2 Test Case and Experimental Data

An experimental data set from tests with the RAE M2129 S-diffuser model provided by QinetiQ was used for the assessment of the numerical simulations. This model, developed at the Royal Aircraft Establishment (a predecessor of QinetiQ), has been tested extensively and widely used for CFD code calibrations.

### 2.1 RAE M2129 S-Diffuser Geometry

The geometry of the M2129 diffuser configuration is shown in Fig. 1. The diameter of the capture area (highlight entry diameter) is 0.144 m (capture area 0.01628686 m<sup>2</sup>). With the throat diameter being equal to 0.1288 m (throat area 0.0130295 m<sup>2</sup>) a contraction ratio of 1.25 is established. The diameter of the engine face is 0.1524 m (engine face area 0.0182415 m<sup>2</sup>) leading to an area ratio between the engine face section and the throat section of 1.4. The offset of the model resulting from the center line curvature is 1.065 times the throat diameter and the length of the duct is 4.668 times the throat diameter. The duct has an upstream lip and parallel extension as well as a downstream parallel extension that includes the engine face

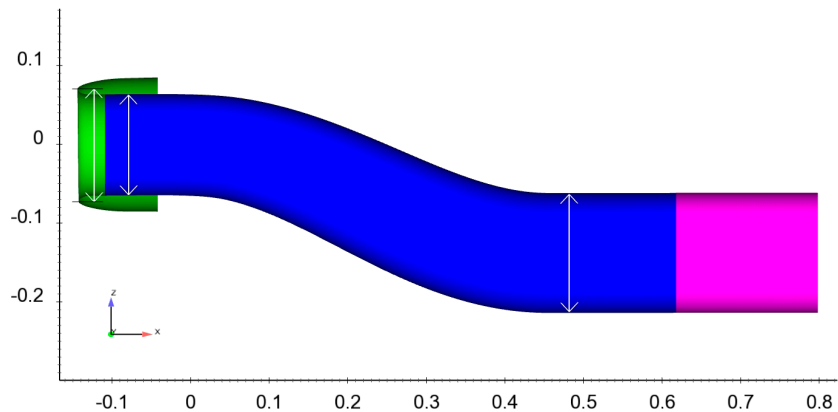


**Figure 1: Geometry of the RAE M2129 S-Shaped diffuser configuration.**

and the outflow boundary domain. The intake duct is curved between the x-positions 0 m and 0.4572 m. The engine face position is located at x = 0.4839 m. The maximum external diameter of the intake is 0.16868 m.

Two variants of the geometry were considered for the GARTEUR AD/AG-43 investigations, one with a bullet and a static rake in the compressor entry plane, as well as one without a bullet and with an engine face rake for unsteady measurements. This paper comprises only results for the geometry without bullet since emphasis was put on the DES computations and unsteady data were only recorded for this variant of the geometry.

### 2.2 Experimental Data for Comparison with Numerical Results

Figure 2 summarizes the experimental data considered for the numerical investigations.

The mass flow ratio (MFR) is defined as  $A_o/A_c$  where  $A_o$  is the cross section area of the captured stream tube at infinity, and  $A_c$  is the intake highlight or capture area.

PRA is the average static pressure at the engine face, non-dimensionalized by the free stream total pressure,  $H_\infty$ . HRA is the total pressure recovery, defined as  $H_{ef}/H_\infty$ , where  $H_{ef}$  is the area-weighted average total pressure at the engine face. DC60 is the static distortion coefficient, defined as:

$$DC60 = \frac{H_{ef} - H_{60min}}{Q_{ef}}$$

where  $Q_{ef}$  is the mean dynamic head at engine face and  $H_{60min}$  is the mean total pressure in the worst 60 deg sector of the engine face.

The dynamic engine face rake has 8 equally spaced arms, each with 5 Pitot pressure probes (see Fig. 2). The arms are at 45 deg intervals. The radii of the probe positions are spaced in an area-weighted manner.

<b>Flow Conditions:</b>	
Free stream Mach Number	0.207
Free stream Total Pressure	103011.2 Pa
Free Stream Total Temperature	282.6 K
Angle of Attack	0°
Angle of Sideslip	0°
Mass flow ratio $A_o/A_c$	2.0425
<b>Engine Face Results (Time-Averaged)</b>	
Engine Face Mach Number	0.395
$PRA = P/H_\infty$	0.8701
Total Pressure Recovery HRA	0.9798

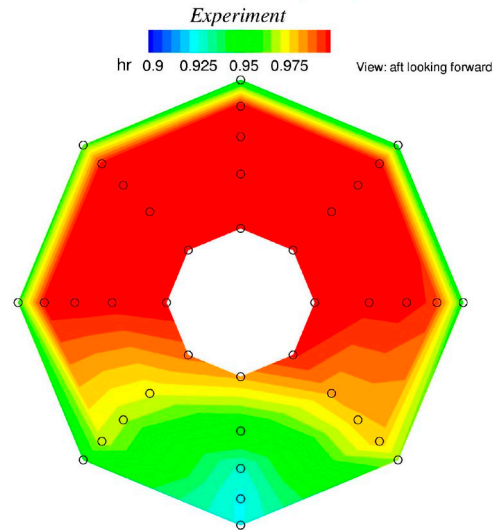


**Figure 2: Experimental data and total pressure contours at engine face with probe positions (circles).**

### 3 Grid Generation, Boundary Conditions, and Numerical Methods Applied

#### 3.1 Grid Generation

For DES a strong link exists between the computational grid and the ability of the method to correctly handle the varying turbulent length scales. The density of the mesh has to be high enough to allow for capturing physical flow phenomena in the separated area downstream of the S-bend.

The structured grid was generated with ICEM CFD based on previous experiences with mesh quality and refinement from URANS calculations for the same diffuser geometry.

The far field upstream of the duct inlet entry and in the lateral direction around the cowl has an extension of about 10 times the duct diameter. The free stream computational domain has a round shape and an O-H-grid-structure was established in order to best fit the geometry. Fig. 3 illustrates the computational domain together with the intake geometry and the mesh density for a cross-sectional cut at the engine face.

In order to apply an outlet boundary condition far enough from the experimental measurement section (engine face) a downstream extension was added to the outlet of the S-duct, keeping the outlet cross section constant over approximately one S-duct length with gradual but rapid coarsening of the grid up to the outflow boundary. The vortices being formed in the shear layer should be destroyed before reaching the outlet plane, so that the outlet boundary condition can remain steady. To achieve the downstream deletion of the vortices, the cell size in the longitudinal direction was increased. For the evaluation of the results, the original compressor entry plane is kept as a block boundary and all vertices lie in the same plane. Since the flow in the engine face plane should not be influenced by the flow immediately downstream, the cell size in the longitudinal downstream direction increases gradually with a ratio of 1.1 along one engine face radius on approximately 20 cells in the x-direction. Further downstream a rapid increase of cell size is realized up to the outflow plane.

The mesh has a multigrid level three capability. A uniform circumferential distribution of grid lines within the near wall blocks results in a very uniform and homogeneous mesh in cross sections of the diffuser duct. The near wall O-grid has 65 nodes, the spacing for the first grid cell above the surface is 0.005 mm, and the ratio for the succeeding grid points on the edges of the near wall blocks is 1.1. Concerning the quality of the mesh, the

determinants for the grid cells are all greater than 0.53. The number of total nodes for the grid is 6,194,145 with 6,129,664 total hexahedral elements.

A refinement of the grid was also performed for investigations regarding grid dependency and for further adaption of the mesh to the requirements of the DES computations leading to approximately 13 million nodes. In order to better capture the development of instabilities in the mixing layer a refined mesh particularly in the transversal direction of the anticipated shear-layer might be beneficial.

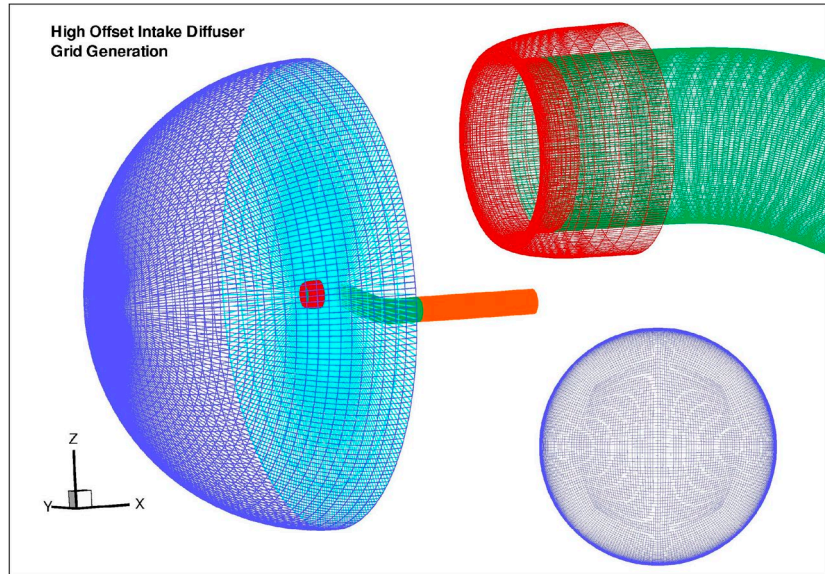


**Figure 3: High quality grid and computational domain for the RAE M2129 diffuser.**

For URANS computations a structured O-H-grid with 1,332,157 nodes was applied, and for RANS computations only one half of the grid was used.

### 3.2 Boundary Conditions

The boundary conditions for the numerical test case, which was investigated, are described by the following parameters:

Mach Number	= 0.207	Static pressure at infinity	= 100018.8 N/m <sup>2</sup>
Angle of Attack	= 0°	Static temperature at infinity	= 280.2 K
Angle of Sideslip	= 0°	Density at infinity	= 1.243745 kg/m <sup>3</sup>
Reynolds Number	= 4932254/m	Diffuser air mass flow	= 2.8727 kg/s

At the outflow plane either a constant static back pressure was applied or a constant mass flow boundary condition was used. When a constant back pressure was applied, the pressure value was adjusted in an iterative manner until the computed mass flow matched the experimental one. At the walls no-slip adiabatic boundary conditions were used.

### 3.3 Numerical Methods Applied by FOI

FOI applied their unstructured in-house CFD solver EDGE for the simulations. EDGE is a node-based compressible Navier-Stokes solver system using a finite volume method.<sup>9</sup> In RANS computations the convective flux is approximated with a second-order central scheme for the Navier-Stokes equations, and a second-order upwind scheme of Roe’s flux difference splitting type is employed for the turbulence transport equation. In the DES modeling, the second order central scheme has been used for the convection terms in both the momentum and turbulence transport equations. The viscous flux has been estimated using a second-order approximation. The time-dependent simulation is advanced using a dual-time stepping method, where a global physical time step is employed and a local time step (the pseudo time step) is used in the sub iterations based on an explicit three-stage Runge–Kutta scheme.

The DES approach by Spalart, Jou, Strelets, and Allmaras<sup>10</sup> has been used, in which the maximum cell size is estimated using the maximum edge of a node.<sup>11</sup> For comparison, RANS computations have also been conducted using the Spalart-Allmaras (S-A) one-equation model,<sup>12</sup> and the  $k-\omega$  EARSM turbulence model.<sup>13</sup>

The fine DES grid with about 6.13 million nodes was used in the computations with the S-A RANS and DES models, while the EARSM computation has been conducted on the coarse RANS grid with about 1.3 million nodes. In the DES computation, two different time steps have been tested, namely,  $\Delta t = 5.0 \cdot 10^{-6}$  s and  $\Delta t = 2.0 \cdot 10^{-5}$  s with no major difference found. The results presented here were obtained with  $\Delta t = 2.0 \cdot 10^{-5}$  s with a statistical sampling time frame of about five cycles of air going through the duct.

### 3.4 Numerical Methods Applied by ONERA

Concerning the steady and unsteady RANS computations ONERA used the elsA in-house code which is a cell-centred finite volume software solving the 3D RANS equations on multi-block structured grids.

The Navier-Stokes equations and the turbulence transport equations were solved separately. Indeed the RANS equations were solved with the Jameson scheme, whereas a Roe scheme with a Harten coefficient of 0.01 was used to solve the turbulence transport equations.

At convergence, the two viscosity parameters for Jameson centered flux were the following:

- $Ki2 = 0.5$  and  $Ki4 = 0.016$  for K- $\omega$  Kok and k- $\epsilon$  J-L computations;
- $Ki2 = 0.5$  and  $Ki4 = 0.032$  for the k-kl EARSM computations.

The LU-RELAX implicit method was used.

Concerning the time integration, a backward-Euler scheme was used for RANS computations whereas a Gear integration was employed for the URANS calculations. Furthermore a local timestep was used in the steady case whereas unsteady computations were performed using a 5.10-6s global timestep with 5 sub-iterations.

RANS and URANS numerical simulations were performed using three different two-equation turbulence models: the k- $\omega$  model of Kok, the k- $\epsilon$  model of Jones-Launder and the k-kl EARSM turbulence model. The k- $\omega$  and k- $\epsilon$  computations are based upon the Boussinesq assumption whereas the k-kl computations were performed with an EARSM (Explicit Algebraic Reynolds Stress Model) formulation using the Wallin-Johansson approach.

The general procedure was to run a succession of RANS computations, adjusting the outflow pressure in an iterative manner until the experimental MFR ("A0AC") was achieved. This output flow was then used in the subsequent URANS calculations.

Concerning the ZDES computations ONERA used the FLU3M in-house code, which is a cell-centered finite volume software solving the 3D RANS equations on multi-block structured grids. The turbulence model implemented in the FLU3M code was originally based on the Spalart-Allmaras RANS model which solves a one-equation turbulence model for the pseudo-eddy viscosity  $\tilde{\nu}$ :

$$\frac{D\tilde{\nu}}{Dt} = c_{b1}\tilde{S}\tilde{\nu} + \frac{1}{\sigma} \left( \nabla \cdot ((\nu + \tilde{\nu})\nabla \tilde{\nu}) + c_{b2}(\nabla \tilde{\nu})^2 \right) - c_{w1}f_w \left( \frac{\tilde{\nu}}{d} \right)^2$$

The eddy viscosity is defined by:  $\mu_t = \rho \tilde{\nu} f_{v1}$ ,  $f_{v1} = \frac{\chi^3}{\chi^3 + c_{v1}^3}$ ,  $\chi = \frac{\tilde{\nu}}{\nu}$

The  $f_w$  and  $f_{v1}$  functions are near-wall damping functions of the model. In Ref. 12 details are given about the constants and the quantities involved. What is important here is that the model is provided with a destruction term for the eddy viscosity that contains  $d$ , the distance to the closest wall. This term when balanced with the production term adjusts the eddy viscosity to scale with the local deformation rate  $\tilde{S}$  producing an eddy viscosity given by:  $\tilde{\nu} \propto \tilde{S}d^2$

Following these arguments, Spalart et al. suggested to replace  $d$  with the new length scale  $\tilde{d}$  given by:

$$\tilde{d} = \min(d, C_{DES}\Delta) \text{ with } \Delta = \max(\Delta_x, \Delta_y, \Delta_z)$$

where  $\Delta$  is the computational mesh size. In the attached boundary layer, due to the significant grid anisotropy ( $\Delta_x \sim \Delta_z \gg \Delta_y$ ) typical of this flow region,  $\tilde{d} = d$  and the model reduces to the standard S-A RANS model. Otherwise, once a field point is far enough from walls ( $d > C_{DES}\Delta$ ), the length scale of the model performs as a Smagorinsky like subgrid-scale version of the S-A model.

Standard DES, however, introduces a significant dependency on the RANS part of the simulation, which requires a grid spacing for the wall grid in tangential direction larger than the boundary layer thickness at that location. This grid resolution may be easily violated inside the duct. If the switching to LES mode occurs inside the RANS boundary layer, this will result in an underestimation of the skin friction coefficient.<sup>14</sup> In order to get rid of a grid induced separation a modification of the model length scale was proposed in Ref. 15 presented as a Delayed Detached Eddy Simulation (DDES) to delay the switch into the LES mode and to prevent "model-stress depletion". As a modification a Zonal Detached Eddy Simulation (ZDES) approach was introduced in Ref. 16, in which RANS and DES domains are selected individually. The motivation is to be fully safe from "model-stress depletion" and grid induced separation and to clarify the role of each region. Significant improvements of the original ZDES method have been recently developed at ONERA. These latter developments have not been used in the frame of the present work but are currently assessed in the GARTEUR Aerodynamics Action Group AD/AG-49.

A local time-step was used for the RANS computations whereas DES computations were performed applying a global time-step size of  $5.0 \cdot 10^{-7}$  s with 4 sub-iterations.

### 3.5 Numerical Methods Applied by NLR

NLR applied their hybrid method X-LES (eXtra-Large Eddy Simulation) for the diffuser flow simulations. The composition of the RANS and LES formulations in X-LES is formed with RANS closed with the turbulent/non-turbulent  $k-\omega$  turbulence model, LES closed with the sub-grid scale model and an implicit switch between RANS and LES, depending on the RANS length scale and LES filter width. RANS will predominantly be applied in the near wall regions where the turbulent length scales are smaller. LES, inversely, is preferably used in regions with more uniform properties, larger turbulent length scales and especially where more physical relevance is required.

Due to the different turbulence modeling approaches, there are main differences between RANS and X-LES. LES resolves the larger scales of the flow, modeling only the smaller scales. RANS does not explicitly resolve any scales, but calculates the mean quantities, which are predominantly determined by the macro-structure, and models the turbulent scales. As LES explicitly resolves turbulent scales in the flow, the produced eddy viscosity will be smaller in LES than in RANS. In LES-mode, this reduces the viscous dissipation and diffusion in the flow, allowing weaker flow structures to sustain in the solution. In RANS the turbulence model is based on flow quantities and is similar for every grid, while for the present study of X-LES, the filter width is directly dependent on grid-spacing. This means that grid-refinement in X-LES not only influences the numerical accuracy, but also the subgrid-scale turbulence model. Thus for X-LES, unlike RANS, grid-refinement past a point of convergence will not deliver the same solution.

The flow simulations for the M2129 S-duct were performed with the flow solver ENSOLV,<sup>17-19</sup> which is part of NLR's flow simulation system ENFLOW. ENSOLV is suitable for simulations of 3D, steady or time-dependent, compressible flows on multi-block structured grids for arbitrary configurations. ENSOLV employs the non-dimensionalized time-dependent Navier-Stokes equations discretized in space using a finite volume method, guaranteeing that the dependent variables are conserved across each cell. In ENSOLV, the steady flow equations (RANS) are solved by an explicit second order conditionally stable Runge-Kutta scheme, and since time-accuracy is not required here, local time-stepping (determining the time-step for each cell separately) and residual averaging (smoothing the high frequency modes, allowing larger time-steps) are applied to accelerate convergence.

The unsteady flow equations (X-LES) are solved by the unconditionally stable dual-time stepping method of Jameson. The essence of the dual time stepping method is to consider the flow equations as a steady state problem in four-dimensional space-time, which has to be solved in pseudo-time at each physical time-step.

Adequate convergence in pseudo-time guarantees the stability in physical time. For each physical time step 50 subiterations were found to be necessary. The physical time is integrated using second-order backward differences. The pseudo-time is integrated by a conditionally stable fourth order finite volume scheme and a second order line-implicit scheme (making the integration normal to the wall implicit, allowing for larger time-steps without adding additional artificial diffusion) near the walls to accelerate local convergence. At NLR hybrid RANS-LES methods have been constantly improved since the finalization of GARTEUR AD/AG-43.

The grid used for the computations consists of two multi-grid levels, denoted "fine" and "medium". These grid-levels have approximately 6 and 0.75 million cells, respectively. Time-steps applied for X-LES-medium and X-LES-fine simulations on respectively the medium and fine grid level of the M2129 grid are  $4.3189 \times 10^{-5}$  s and  $2.1594 \times 10^{-5}$  s.

### 3.6 Numerical Methods Applied by EADS Cassidian

EADS CASSIDIAN applied the finite-volume DLR-TAU-Navier-Stokes Code<sup>20</sup> for the DES flow field computations with a Spalart-Allmaras<sup>12</sup> turbulence model. The code employs an unstructured spatial flow field discretization and dual-time stepping scheme for time-accurate (unsteady) calculations. A brief general description of the flow solver is provided below. Further details are given in Ref. 20.

For a generated primary grid, pre-processing needs to be employed once, which computes the dual grid composed of general control volumes from the primary elements. They are stored in an edge based data structure, which leads to the independence of the solver from the primary grid element types. All metrics are given by normal vectors, representing size and orientation of the faces, the geometric coordinates of the grid nodes and the volumes of the dual cells.

The code solves the compressible governing equations using vertex-centered metrics with second-order spatial and temporal accuracy. Inviscid fluxes are computed employing either a second-order central differencing scheme or a variety of upwind schemes with second-order accuracy. Viscous terms are computed with a conventional second-order central differencing scheme. Either scalar or matrix artificial dissipation may be chosen by the user in order to stabilize the convective central difference operators.

For time-accurate calculations both dual time-stepping (Jameson) and global time-stepping techniques are supported. Various acceleration techniques are applicable like multi-grid algorithms and explicit as well as implicit residual smoothing. In the dual-time-stepping approach the time derivatives are first discretized by a second-order backward difference formula and the resulting sequence of non-linear steady-state problems is solved in pseudo-physical time by an explicit Runge-Kutta or an implicit lower-upper symmetric Gauss-Seidel (LU-SGS) algorithm, until a steady state in pseudo-time is reached. Compared to the explicit Runge-Kutta method, the LU-SGS scheme is stable with almost no time step restrictions. In terms of iterations LU-SGS can be seen to converge approximately twice as fast as the Runge-Kutta scheme. Furthermore, one iteration of LU-SGS costs roughly 80% of one Runge-Kutta step. This results in a reduction of the overall calculation time by a factor of 2.5.

DES is a non-zonal hybrid RANS-LES method, and for the Spalart-Allmaras variant (S-A DES) used in the present work the switching between the RANS and LES modes is controlled by the wall distance. This approach combines RANS modeling near solid walls where a LES type resolution of the flow is too expensive, and LES distant from the walls where flow separation occurs and a RANS formulation is not consistent with the flow physics. The switch between RANS and LES modes is based on a modified definition of the characteristic length scale in the Spalart-Allmaras<sup>12</sup> turbulence model, depending on the distance from the wall and the largest edge length of the local grid cell.

In order to investigate the impact of the time step size on the numerical results three different time steps were applied:  $\Delta t = 2.0 \cdot 10^{-5}$  s,  $\Delta t = 5.0 \cdot 10^{-6}$  s, and  $\Delta t = 5.0 \cdot 10^{-7}$  s.

## 4 Numerical Results

Since the performance of DES computations for the RAE M2129 diffuser was the major subject of the GARTEUR Aerodynamics Action Group AD/AG-43 emphasis is laid on the illustration of the DES results within the present paper. For the comparison with DES simulations RANS and URANS computations were performed. A selection of these numerical data is presented. More detailed results are available in Ref. 21.

For an assessment of the flow field, sectional cuts through the three-dimensional flow field were made. Time-averaged values are based on several thousand physical time steps. Instantaneous values are given for the last time-step of the computations.

### 4.1 Numerical Results of RANS and URANS Computations

RANS computations for the M2129 configuration were performed with one half of the structured O-H-grid with approximately 1.3 million nodes. For the URANS simulations the complete computational model was applied in order to assess the influence of the unsteadiness of the flow. To avoid erroneous inclusion of start-up transients in the data analysis, the first five characteristic time periods (convection time for the flow from intake entry to engine face) of the unsteady CFD time history were discarded. The averaging of the flow properties was carried out over eight succeeding characteristic periods.

In the present paper numerical results for the  $k-\omega$  Kok and the  $k-kl$  EARS turbulence models are shown. Ref. 21 also comprises computational data for the  $k-\epsilon$  Jones-Launder turbulence model.

Table 1 presents a comparison of the time-averaged integrated parameters between experiment and RANS/URANS simulations. For the computations the mass flow through the duct could in general be kept within a margin of 0.8% in comparison with the experiment with the exception of the URANS computation applying the  $k-\omega$  Kok model with a larger difference of -1.33%. The stream tube area ratio corresponding to the mass flow is about two. Computed Mach numbers in the compressor entry plane are in the order of 0.42 and thus represent realistic magnitudes. Mach number deviations of the numerical results from the experimental data are in the range between 5% (URANS  $k-\omega$  Kok model) and 9% (RANS  $k-kl$  EARS model).

The computed values of total pressure recovery and flow distortion highly depend on the turbulence modeling. While the total pressure recovery (HRA) is within 0.1% of the experimental value when performing a RANS computation with the  $k-\omega$  Kok model, it is underestimated when using the  $k-kl$  EARS model (-1.8%). Similarly the distortion parameter differs widely according to the turbulence model: +37% with the  $k-\omega$  Kok model and +126% with the  $k-kl$  EARS model.

Table 1 highlights the improvement of the flow distortion prediction obtained when performing a URANS computation (with a global time step of  $5 \times 10^{-6}$  s and 5 sub-iterations) instead of a RANS computation (using a local time step) even if the predicted values greatly differ from the experimental results. More precisely, the DC60 parameter evolves as follows when performing an unsteady computation instead of a steady one: +28% instead of +37% with the  $k-\omega$  Kok model, +73% instead of +126% with the  $k-kl$  EARS model.

**Table 1 RANS and URANS computational results for the M2129 duct for different turbulence models and comparison with experimental data (elsA code).**

	Experiment	RANS	URANS	RANS	URANS
Turbulence Model	-	k- $\omega$ Kok	k- $\omega$ Kok	k-kl EARSM	k-kl EARSM
Outlet pressure (Pa)	-	89050	89050	87150	87150
Mass flow (kg/s)	2.873	2.866	2.834	2.861	2.874
$\Delta$ Mass flow/Mass flow	-	-0.22%	-1.33%	-0.41%	0.05%
<b>Ao/Ac</b>	<b>2.043</b>	<b>2.074</b>	<b>2.028</b>	<b>2.064</b>	<b>2.047</b>
$\Delta$ (Ao/Ac) / (Ao/Ac)	-	<b>1.53%</b>	<b>-0.72%</b>	<b>1.05%</b>	<b>0.23%</b>
Mach in the CEP	0.3950	0.4234	0.4141	0.4313	0.4264
$\Delta M_{ef} / M_{ef}$	-	+7.2%	+4.8%	+9.2%	+7.9%
PRA	0.8701	0.8613	0.8621	0.8356	0.8409
$\Delta$ PRA / PRA	-	-1.0%	-0.9%	-4.0%	-3.4%
$\eta_{02} = \text{HRA}$	<b>0.9798</b>	<b>0.9806</b>	<b>0.9760</b>	<b>0.9620</b>	<b>0.9627</b>
$\Delta \eta_{02} / \eta_{02}$	-	<b>0.1%</b>	<b>-0.4%</b>	<b>-1.8%</b>	<b>-1.7%</b>
<b>DC60</b>	<b>0.2700</b>	<b>0.3696</b>	<b>0.3455</b>	<b>0.6091</b>	<b>0.4670</b>
$\Delta$ (DC60) / (DC60)	-	<b>37%</b>	<b>28%</b>	<b>126%</b>	<b>73%</b>

To better understand the distortion coefficient discrepancies between experiment and RANS/URANS computations, comparisons of Mach number and total pressure contours are shown in Fig. 4 and Fig. 5. These plots reveal that total pressure levels downstream of the recirculation region are underestimated by all turbulence models and especially by the k-kl EARSM model. Total pressure losses are more pronounced for the RANS computations than for the URANS simulations. Thus it appears that turbulence models encounter difficulties to accurately predict the level and the extension of this low total pressure area. Furthermore, since a slight variation in the level of the minimum total pressure in the CEP leads to a significant difference in the value of the DC60 coefficient, substantial discrepancies appear between the computed and experimental DC60 values. It is consequently extremely difficult to accurately predict the DC60 distortion parameter when flow separation is present.

The time-averaged contours obtained with URANS computations are closer to the experiment than those obtained with steady RANS simulations. When using an unsteady computational approach, the low total pressure region in the engine face decreases, eventually becomes flatter towards the duct center, and results in total pressure levels closer to the experiment. This results from the fact that the recirculation region is less extended when performing an unsteady simulation instead of a steady computation, as the Mach number contours in the symmetry plane and the static pressure distributions along the S-bend reveal (the plateau corresponding to the separated flow area is less extended when using a URANS approach as clearly shown in Fig. 5). A direct consequence is a better prediction of the distortion coefficient when performing unsteady computations (see Table 1).

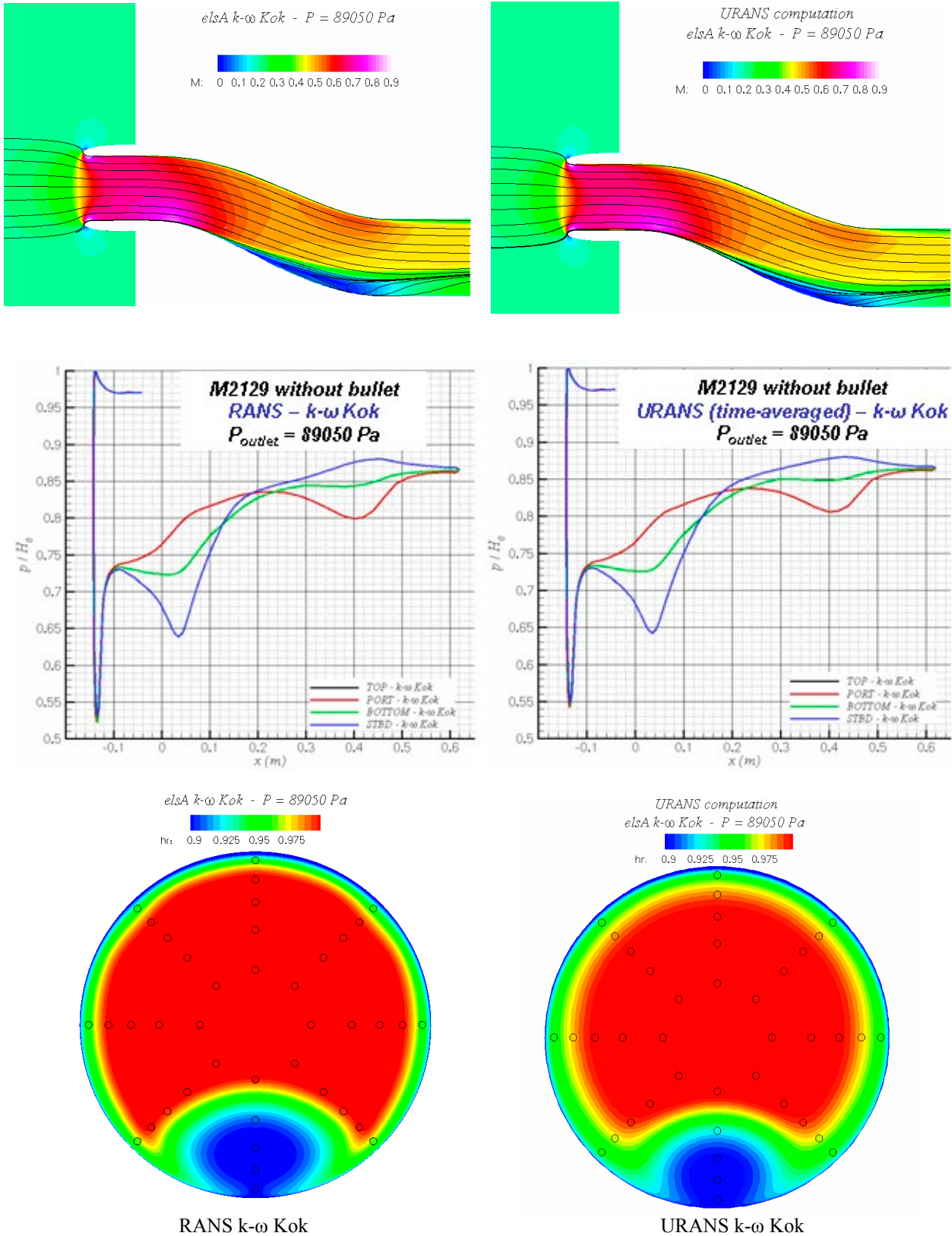


Figure 4: RANS and URANS computations performed with  $k-\omega$  turbulence model of Kok.

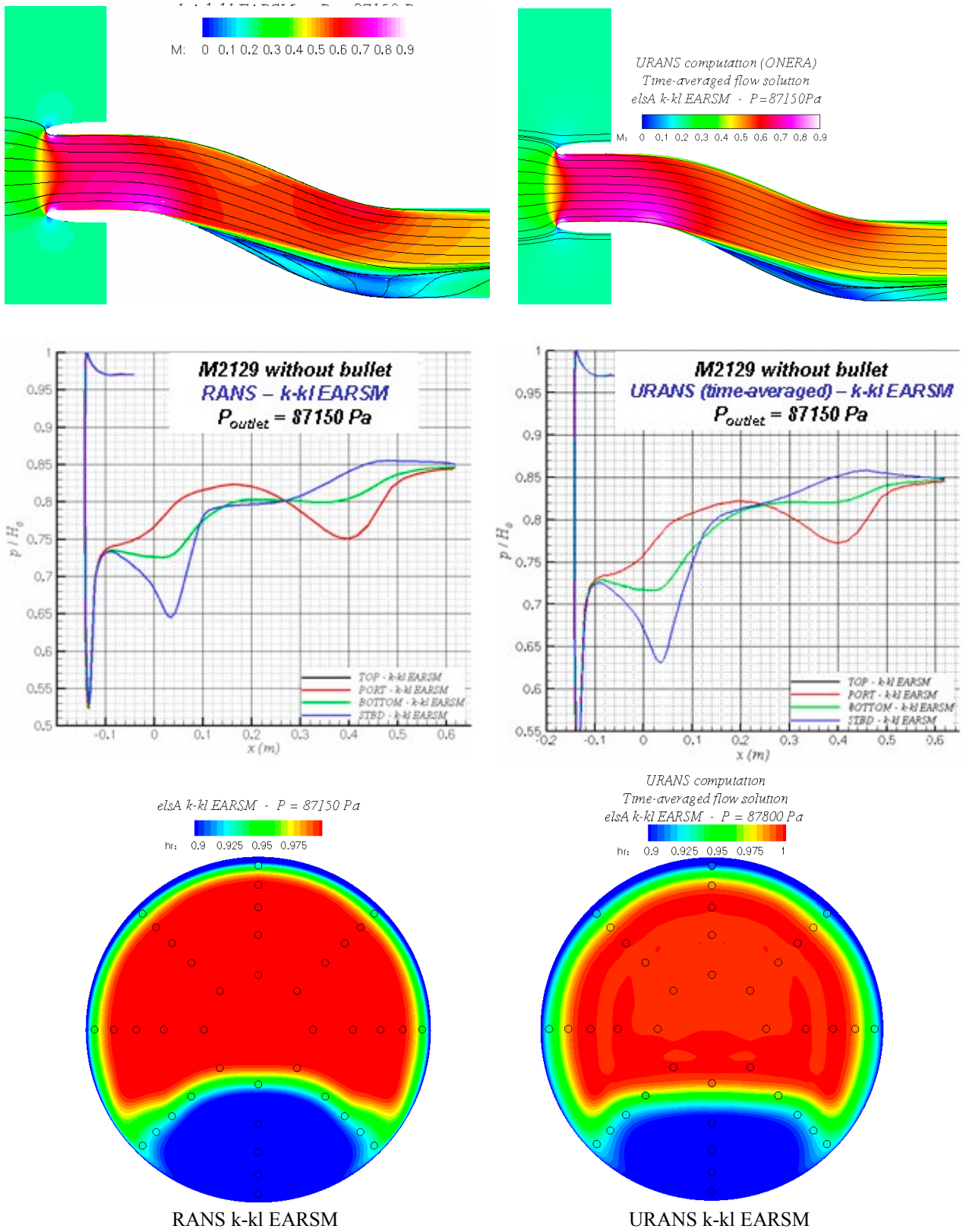


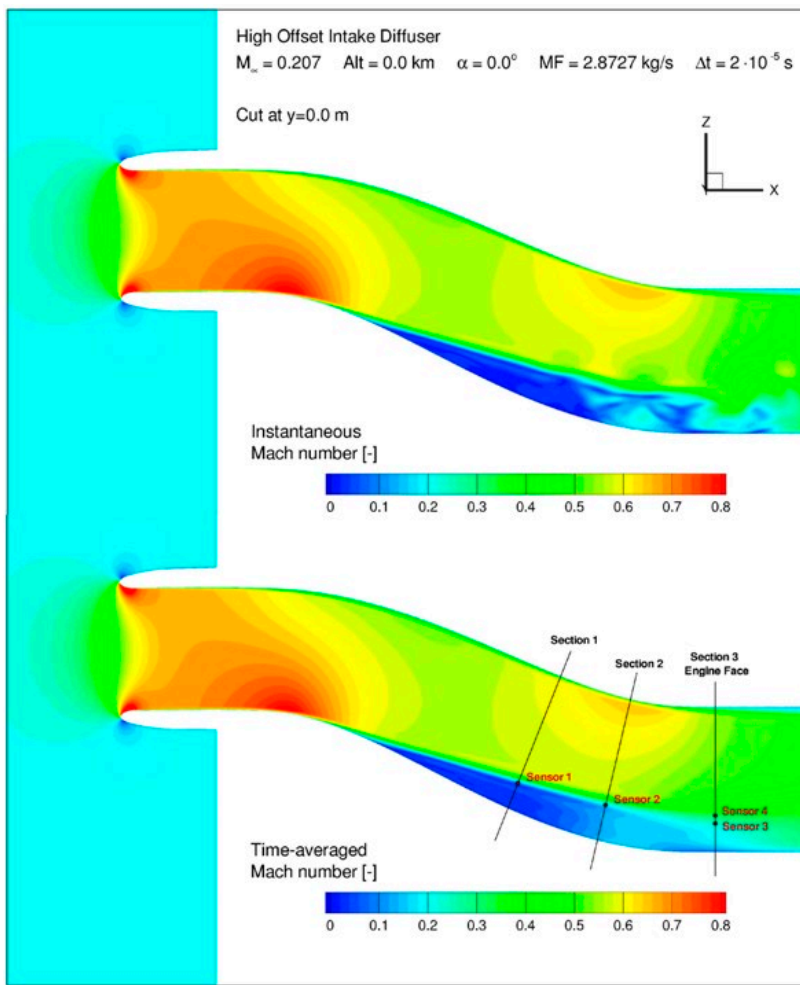
Figure 5: RANS and URANS computations performed with k-kl EARSM.

### 4.2 Numerical Results of DES Simulations

For a first overview of the DES computations of the diffuser flow field, Fig. 6 shows a comparison of the instantaneous and time-averaged Mach number distributions in the symmetry plane illustrating the flow characteristics inside the S-shaped duct. Low Mach numbers (blue color) clearly indicate the large separated flow region on the lower wall of the diffuser. Reattachment of the flow occurs downstream of the S-bend of the duct. Low Mach numbers can be detected at the upper wall, but flow separation does not occur.

While the first part of the separation region appears more or less steady for the instantaneous flow, the second part reveals large eddy turbulence downstream of the bursting.

In Fig. 6 three cross sections (Section 1, Section 2, and Section 3 Engine Face) are marked for which Mach number and total pressure ratio data are compiled in Fig. 7 and Fig. 8 for the time-averaged and instantaneous flow fields. In these figures all views onto the cross-sectional cuts perpendicular to the flow direction are aft looking forward. Section 1 is within an area of the separated flow region where only minor changes between the



time-averaged and instantaneous flow field occur. Further downstream, at section 2, differences between mean and time-dependent parameter distributions are more pronounced. Flow phenomena in the engine face plane, section 3, illustrate the large eddy turbulent character of the separated duct flow. A comparison between the time-averaged Mach numbers as well as the total pressure ratios and the instantaneous flow parameters clearly reveals that peaks of these parameters can occur in the onset flow for the compressor face of the engine. These peaks of the total pressure recovery are especially important, since they are the basis for the calculation of distortion parameters, and obviously cannot be captured by steady computations. Only the knowledge of dynamic distortion parameters can allow a reliable assessment of the engine/intake compatibility behavior for this type of diffuser. At present, instantaneous total pressures due to unsteady flow behavior can only be recorded by expensive wind tunnel experiments in order to provide reliable data for the deduction of dynamic distortion parameters.

**Figure 6: Comparison of instantaneous and time-averaged Mach number distributions in the symmetry plane of the M2129 diffuser.**

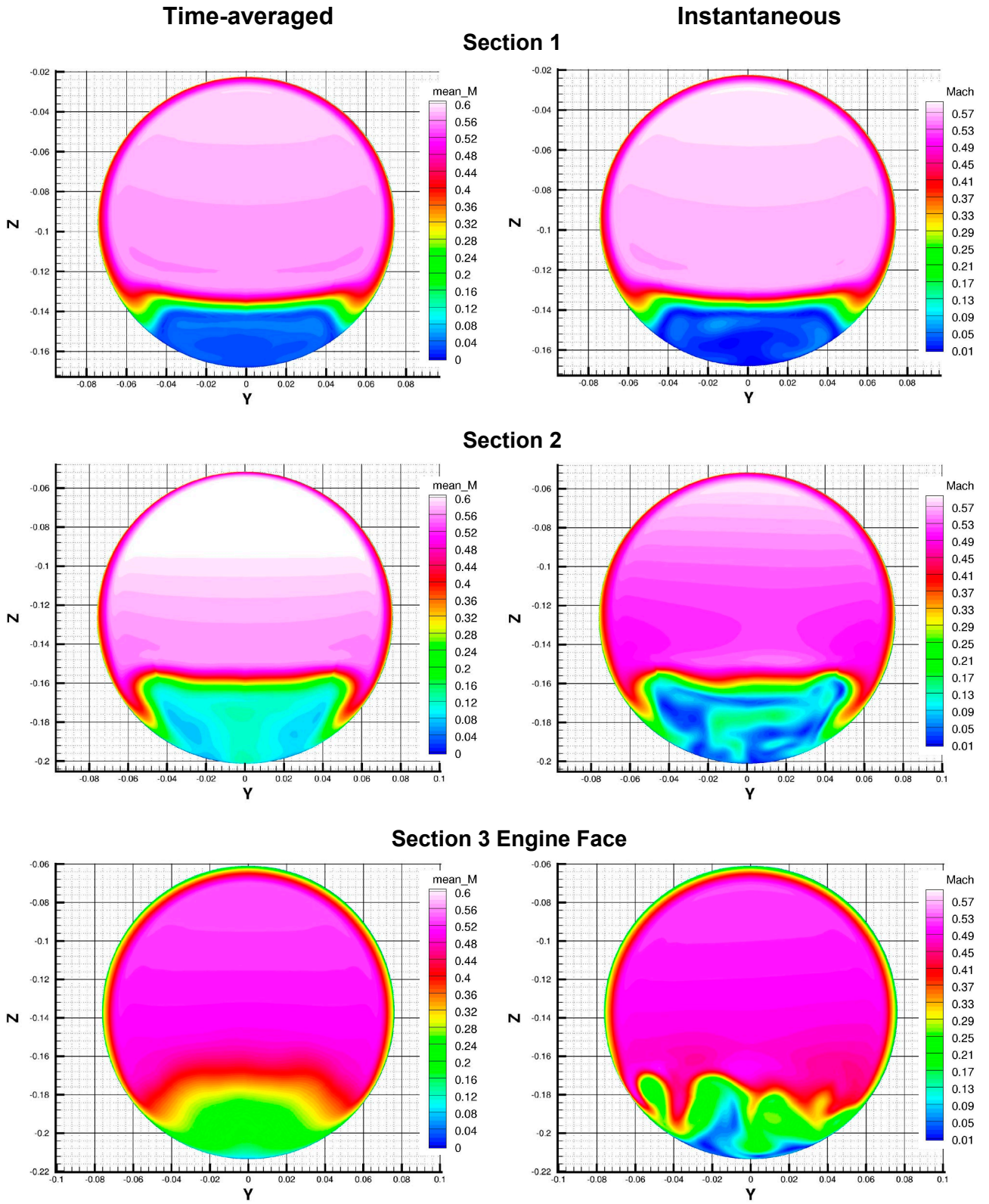
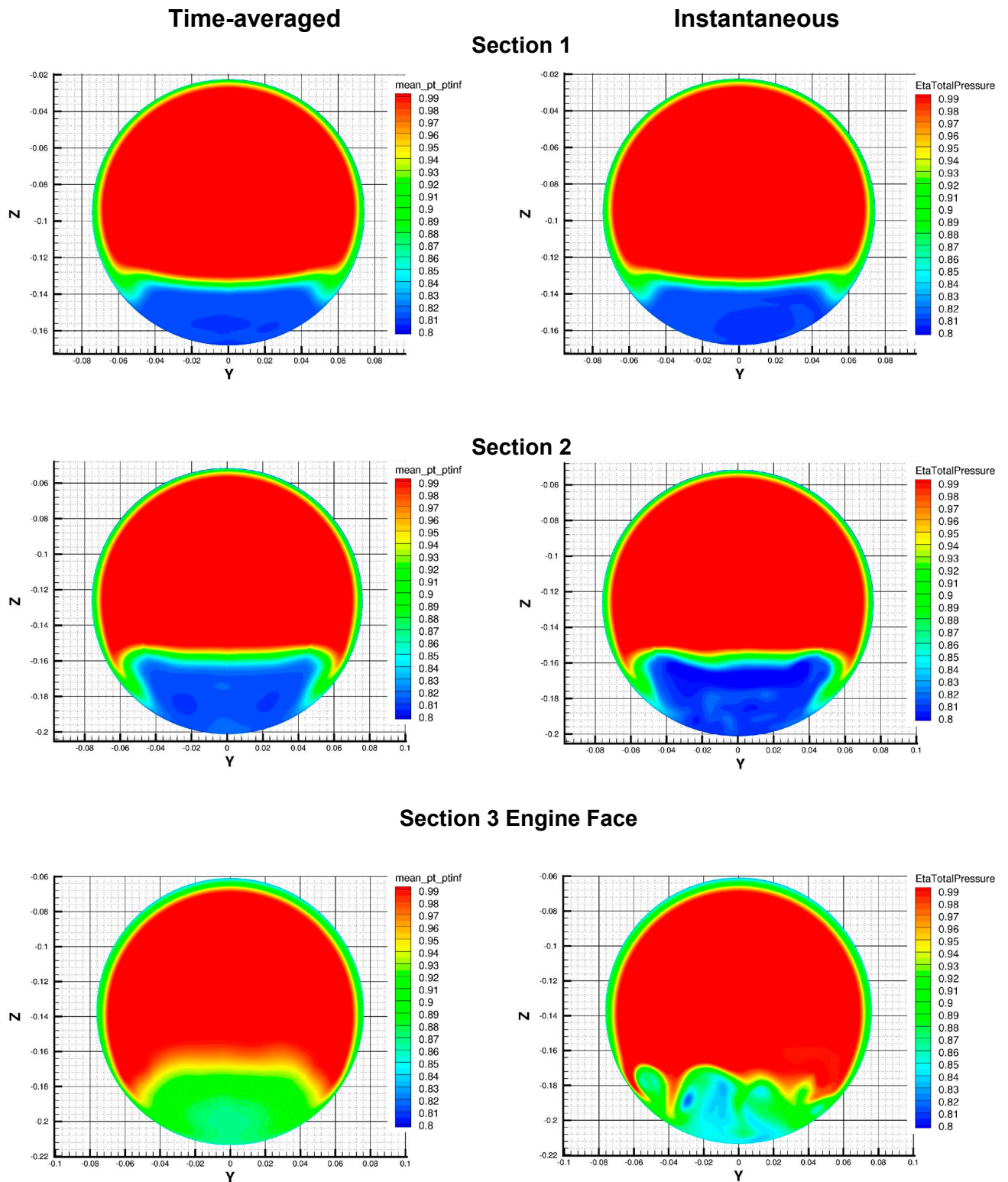


Figure 7: Time-averaged and instantaneous Mach number distributions in three sections (see Fig. 6) of the M2129 diffuser flow field.



**Figure 8: Time-averaged and instantaneous total pressure ratio distributions in three sections (see Fig. 6) of the M2129 diffuser flow field.**

The slight asymmetry of the displayed parameters in the cross sections for the time-averaged values suggest that the total number of physical time steps (for these results 8000) might not quite be enough to ensure an exact description of the mean flow field. A longer time period for statistic analysis to get the averaged mean flow quantities for the DES computation would improve the expected symmetrical flow pattern.

Figure 9 provides a comparison between the eddy viscosity levels obtained with the ZDES computation and the preceding steady RANS calculation which was used to initialize the ZDES computation. In order to avoid erroneous inclusion of start-up transients in the data analysis, the first 10 characteristic time-periods (convection time for flow from highlight to engine face) of the unsteady CFD time history were discarded. The averaging was carried out over 15 further characteristic periods. As illustrated on the ZDES plot, the highest turbulent viscosity levels are observed in the attached boundary-layer regions that are explicitly treated in URANS mode regardless of the grid resolution. In the same figure, it can be noticed that low turbulent viscosity levels are obtained in the shear layer and in the separated flow area handled in LES mode.

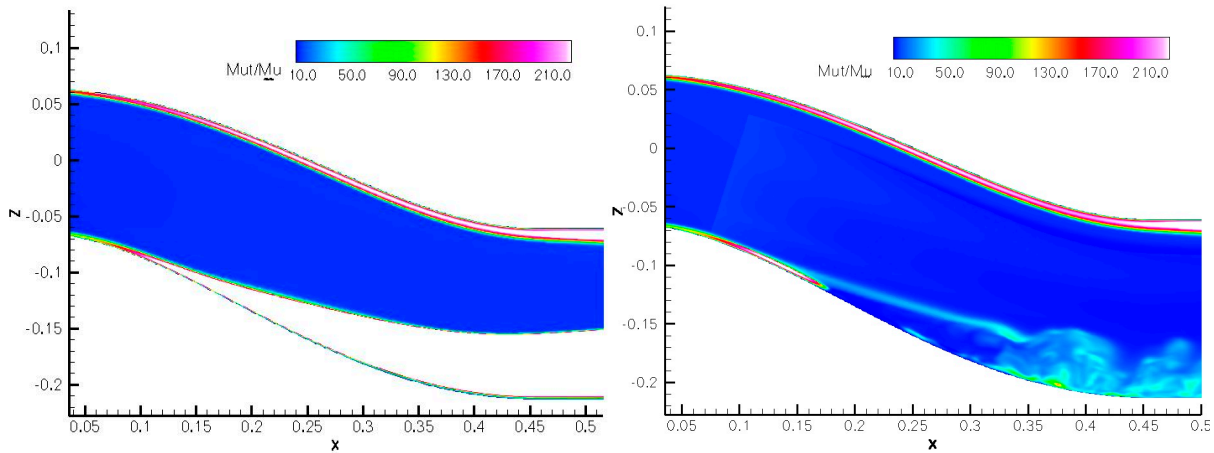


**Figure 9: Comparison of the eddy viscosity level contours obtained with RANS (left) and ZDES (right) computations applying the FLU3M code (refined grid with approximately 13 million nodes).**

RANS computations were also performed with the DES refined grid with approximately 13 million nodes for comparison with the results obtained with the coarser grid.

The ZDES aerodynamic fields are time-averaged during computation before being compared with the experiment (Fig. 2) and the RANS S-A computation (Fig. 10). To make the comparison between experiments and simulations as similar as possible the same extraction for the engine face data has been used as for the experiments. This means that only data from the probe locations (8 equally spaced arms with 5 pitot pressure probes on each) on the rake arms in the experiment have been used to compute the flow characteristics at the engine face.

Wall static pressure distributions along the duct (Fig. 10) show that the ZDES calculation predicts a somewhat earlier and more extended flow separation on the lower wall surface (starboard distribution) with a more extensive separation bubble than a RANS approach. The reattachment location has been moved further downstream. As a result total pressure contours in the CEP (Fig. 10) point out that the ZDES calculation predicts a more extended low-speed area with a larger low pressure recovery zone and consequently a higher distortion coefficient than the RANS S-A computation (Table 2).

The RANS results for the flow parameters (Table 2) are actually closer to the experimental observation than the hybrid data. The discrepancies in the ZDES computations may be attributed to the resolved free shear layer, which has shown undesirably delayed instabilities. Similar predictions for the free shear layer have been



observed by all partners in the present project work applying different DES methods. This may partly be due to the inflow turbulent condition, which might not be appropriately accommodated by the upstream modeling using the current grid resolution in the domain around the duct inlet. Moreover, the delayed instabilities of the free shear layer may also partly be associated to the function of the LES mode incorporated in the DES model. Obviously, the resolved turbulent diffusion by the LES mode of the free shear layer is insufficient, i. e. the modeled eddy viscosity in the free shear layer has been too large.

Concerning the overall coefficients, the total pressure recovery is calculated within 0.7% by all computations (RANS and ZDES). The total pressure recovery is well captured by the Spalart-Allmaras model with a predicted value within 0.3% of the experimental data. The DC60 parameter differs by 40% for the RANS computation due to an underestimation of the total pressure level in the low-speed region of the CEP and by 66% for the hybrid RANS-LES simulation. However, as mentioned before, the distortion parameter which is extremely sensitive to the local flow characteristics is systematically over-estimated, the deviation from the experimental value being higher for the ZDES solution than for the RANS results due to an overestimation of the separated flow region. The latest developments within the ZDES approach (not applied within GARTEUR AD/AG-43) would certainly improve the numerical results since they are especially dedicated to solving the delay in the formation of instabilities. It is obvious that an accurate modeling of the separation bubble over the duct offset is essential to obtain accurate predictions of the flow features at the engine face.

**Table 2. RANS and ZDES computational results for the M2129 duct compared with the experimental data (refined grid with approximately 13 million nodes).**

	Experiment	RANS	RANS/LES
<b>Turbulence Model</b>	-	<b>Spalart-Allmaras</b>	
Outlet pressure (Pa)	-	88300	88300
Mass flow (kg/s)	2.873	2.850	2.820
$\Delta$ Mass flow/Mass flow	-	-0.8%	-1.8%
<b>Ao/Ac</b>	<b>2.043</b>	<b>2.048</b>	<b>2.042</b>
<b><math>\Delta</math>(Ao/Ac) / (Ao/Ac)</b>	-	<b>+0.3%</b>	<b>-0.004%</b>
Mach in the CEP	0.3950	0.4188	0.4195
$\Delta M_{ef} / M_{ef}$	-	+6.0%	+6.2%
PRA	0.8701	0.8607	0.855
$\Delta$ PRA / PRA	-	-1.1%	-1.7%
<b><math>\eta_{02} = HRA</math></b>	<b>0.9798</b>	<b>0.9770</b>	<b>0.9731</b>
<b><math>\Delta\eta_{02} / \eta_{02}</math></b>	-	<b>-0.3%</b>	<b>-0.7%</b>
<b>DC60</b>	<b>0.2700</b>	<b>0.3792</b>	<b>0.4478</b>
<b><math>\Delta</math>(DC60) / (DC60)</b>	-	<b>40%</b>	<b>66%</b>

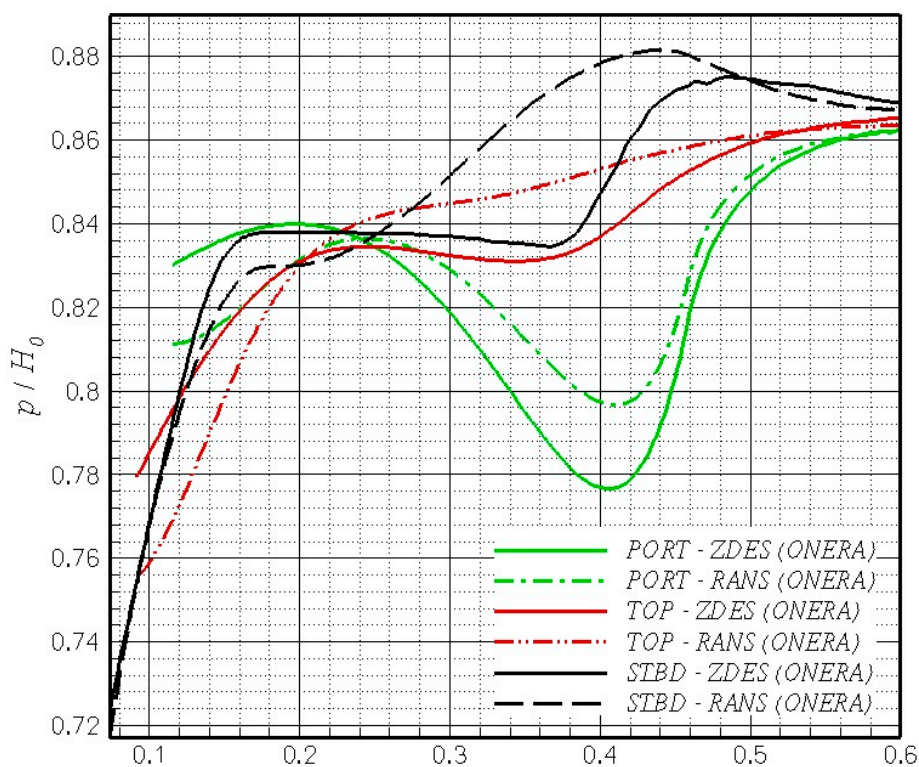
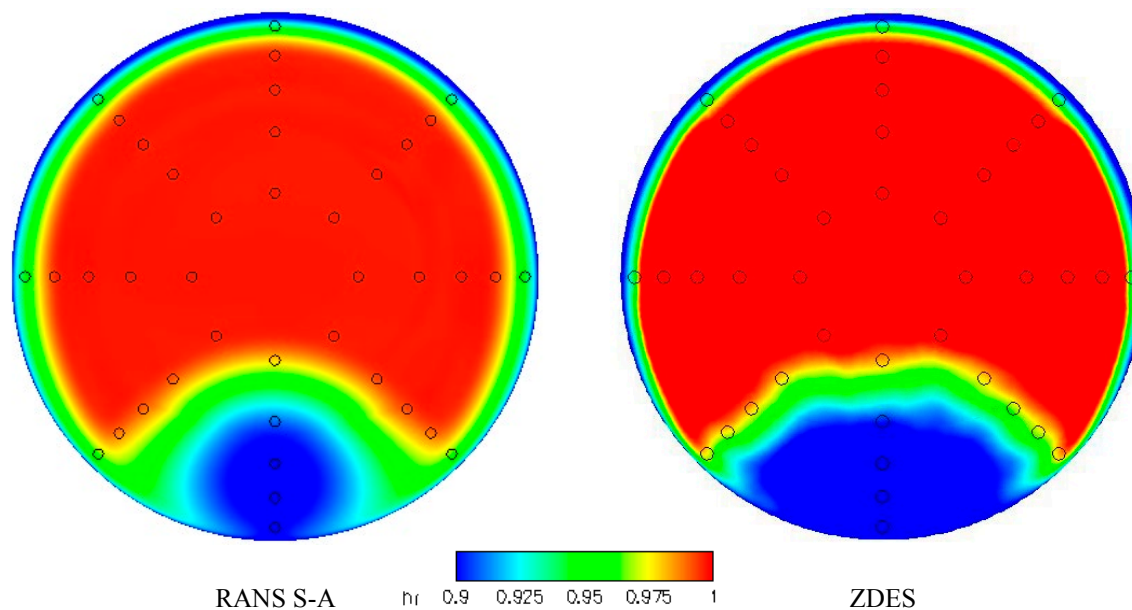


**Figure 10: Comparison of RANS S-A and ZDES computations applying the FLU3M code (refined grid with 13 million nodes): Time-averaged flow solution in the CEP (top) and static pressure distributions along duct walls (bottom).**

Wall streamline topologies are shown for RANS and X-LES-medium simulations in Fig. 11 acquired from the tangential wall shear stress distribution. In all simulation results a topology can be distinguished, which exhibits two saddles (i.e. S1 and S2) and two spiralling nodes (i.e. N1 and N2). Comparing RANS and X-LES, the streak lines near the spiralling nodes, however, differ. In RANS the streak lines are spiralling inwards at N1 and N2, indicating nodes of separation at which a vortex pair leaves the surface. In X-LES, however, the nodes N1 and N2 have increased in size and the direction of spiralling at the nodes is outwards instead of inwards. This indicates a node of attachment or stagnation point flow, at which a recirculating vortex structure reattaches to the surface. This kind of behaviour is also observed in the X-LES-fine solution, which exhibits smaller detailed structures inside the recirculation region compared to X-LES-medium computation.<sup>19</sup> As a consequence of the larger recirculation region predicted in X-LES and the corresponding low pressure in the wake of the recirculation region, vortices are attracted towards the center of the duct. The attraction to the center also leads to an expansion of the shear layer vortices, indicated by the outward spiraling of the vortices. Back-flow of vortical structures in the recirculation region is observed for both X-LES solutions in contrast to RANS. The bifurcation lines (positive (B+) and negative (B-)) visible in the streak line plots of Fig. 11 represent the reattachment and separation of vortices moving downstream.

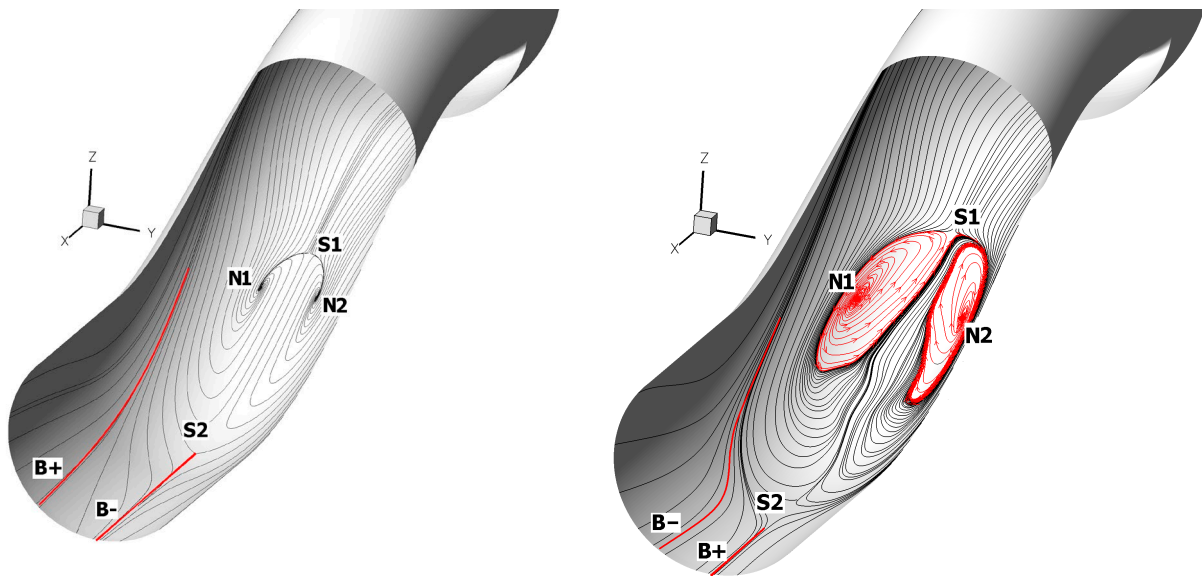


**Figure 11: Wall streamline topologies at the M2129 inlet surface acquired from the wall shear stress distributions for RANS (left) and X-LES-medium (right) simulations.**

The unsteadiness and the time-evolution of the flow field can also be captured by pressure fluctuations for different sensor points (see Fig. 6) in the separated flow region. The time history of the total pressure recovery was recorded for DES computations and is displayed in Fig. 12 for a time period of 0.16 s with the same scale for the total pressure ratio. While sensor 1 at the border between the flow separation and the core flow of the duct shows very moderate fluctuations, sensor 2 further downstream faces much higher amplitudes in total pressure. Sensors 3 and 4 which are located in the engine face plane (section 3), reveal the highly turbulent character of the flow in this cross section with pressure fluctuations of high frequency and relatively large amplitudes of approximately  $\pm 12\%$  relative to the mean value. Further investigations are mandatory in this field to determine resonance frequencies which might cause adverse effects on the vibration behavior of the compressor blades of the engine and could turn out to be harmful to the compressor life.

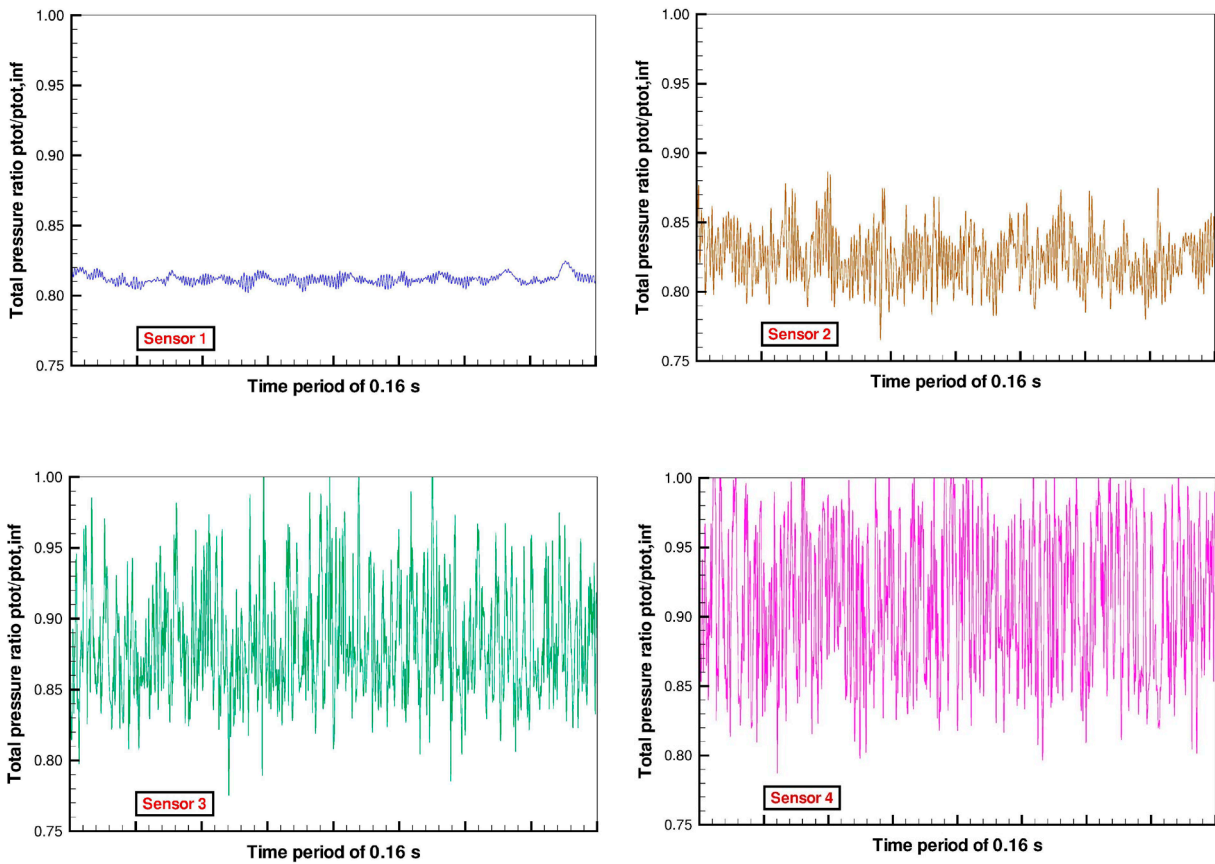


**Figure 12: Total pressure fluctuations in the diffuser flow field at four sensor points (see Fig. 6) of the M2129 diffuser flow field.**

The distortion parameter DC60 for section 3 (engine face) was evaluated for the steady state and dynamic simulations and is displayed in Fig. 13 as a function of time. The initial part of the dynamic history has been discarded due to the transient development of DC60 before the flow has been fully developed. The fluctuations of the air intake performance parameter DC60 are determined by the dynamics of the reattachment process. Roll-up of larger Kelvin-Helmholtz like eddies created in the shear layer and convected towards the engine face as well as smaller three-dimensional flow structures carried back towards the separation zone lead to a feedback mechanism. The time history of the DC60 value is pronounced which suggests that the unsteadiness in the flow downstream of the separation is rather extensive. It is obvious that distortion based on time-averaged values for the total pressures in the engine face does not reflect the dynamic behavior of the flow in a high offset intake diffuser and cannot be used for the assessment of the engine/intake compatibility.

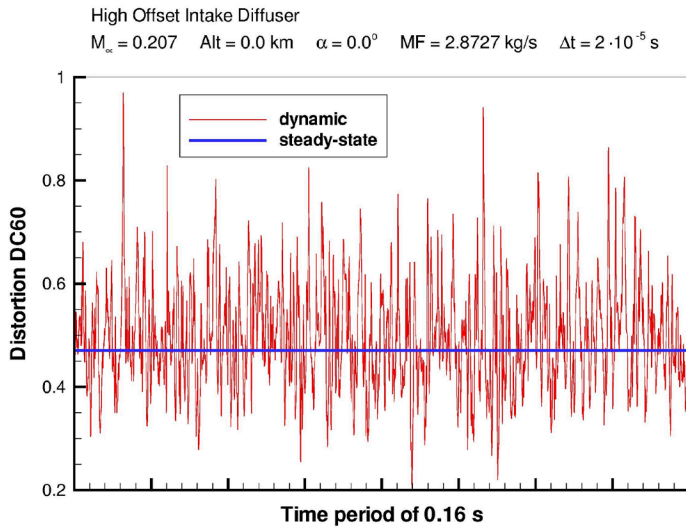


**Figure 13: Distortion parameter DC60 for steady state and dynamic simulations of the intake flow (section 3, engine face).**

Total pressures were recorded at the rake probe locations in the engine face plane (section 3, see Fig. 6) for all physical time steps and the time-averaged values were calculated for these positions. A direct comparison of experimental data with DES results reveals an overprediction of total pressure losses for the numerical simulation. Total pressure recovery is in the order of 5% smaller for the core area where separated flow dominates the flow field structure. The pattern of the region with total pressure losses for the numerical case is in limited accordance with the experimental data.

Figure 14, c) shows the time-averaged total pressure ratio distribution from the DES calculations for the complete engine face (section 3 in Fig. 6) for a comparison with the extracted rake data. The probe positions of the pitot rake are indicated as circles. Since in this case the total pressure recovery for the complete field was processed, as opposed to the local data recording for the rake probes, patterns of the parameter distribution are different. While the distribution in Fig. 14, b) as an interpolation from the specific values at the probe locations cannot account for flow phenomena occurring in the 45 degrees sections between the rake arm positions, a full evaluation of the numerical data for the corresponding flow field delivers a more complete picture. The boundary layer on the upper side of the diffuser duct is more pronounced for the numerical results since total pressure probes do not record the near wall losses due to the required distance of the probes from the walls.

A comparison between experimental rake measurements for the total pressure recovery in the engine face plane (section 3, see Fig. 6) and time-averaged calculated total pressure ratios from the DES simulations is illustrated in Fig. 14. In this figure, the views onto the engine face plane are aft looking forward. The experimental results (Fig. 14, a) show the time-averaged total pressure ratio distribution based on probe values of a dynamic engine face rake consisting of eight equally spaced arms each having five pitot pressure probes (see chapter II, B). The positions of the total pressure probes are shown as circles in Fig. 14.

In Fig. 14, b) DES results are displayed as time-averaged data from 8000 physical time steps with 40 sub-iterations for each time step processed the same way as the experimental data for a direct comparison.

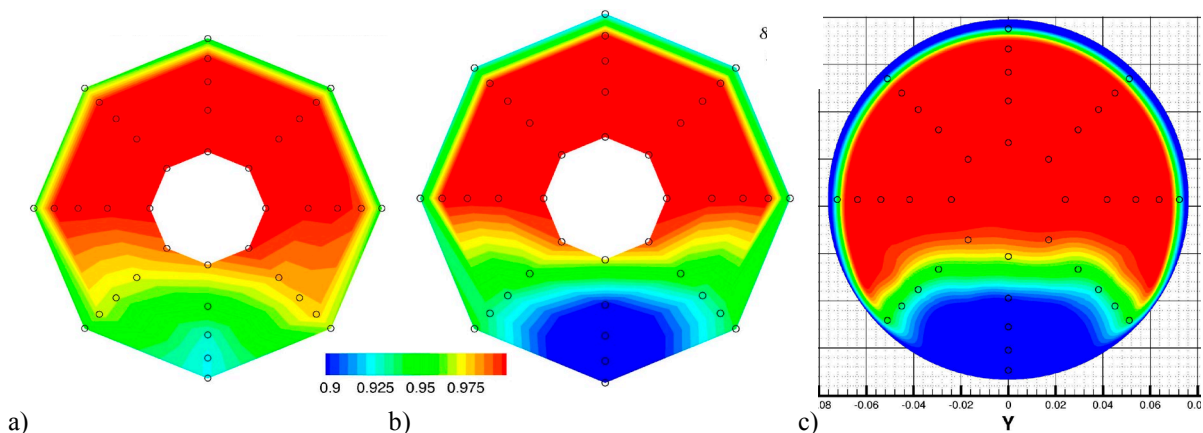


**Figure 14: Total pressure ratio distributions for a) experimental results, b) time-averaged results from DES computation under consideration of data for rake sensor points in section 3 (Fig. 6) only, and c) time-averaged results from DES calculation in section 3 under consideration of complete cross section (DES for 8000 iterations with  $\Delta t = 2 \cdot 10^{-5}$  s, view aft looking forward, rake sensor points are indicated as circles).**

When describing the dynamic distortion with numerical investigations, the physical time step applied to the flow simulation is of major importance. The main objective is to well capture physical flow phenomena occurring with high frequencies like turbulent swirling of the flow in the separation region downstream of the S-bend of the diffuser duct and to quantitatively assess them. When time steps are too large, instantaneous effects will numerically be straightened out and flow phenomena will appear steady. Time steps which are unnecessarily too small will lead to a waste of computer resources.

DES computations with  $\Delta t = 5.0 \cdot 10^{-6}$  s and  $\Delta t = 5.0 \cdot 10^{-7}$  s were performed in addition to a time step size of  $\Delta t = 2.0 \cdot 10^{-5}$  s in order to investigate the impact of the time step on the computational results.

For comparison with Fig. 13, DC60-values for steady state and dynamic simulations of the intake flow (section 3, engine face) are shown for physical time steps of  $\Delta t = 5.0 \cdot 10^{-6}$  s and  $\Delta t = 5.0 \cdot 10^{-7}$  s in Fig. 15. For time steps of  $\Delta t = 2.0 \cdot 10^{-5}$  s and  $\Delta t = 5.0 \cdot 10^{-6}$  s steady state distortion parameters have the same value, and the dynamic data feature the same behavior with similar amplitudes. In contrast, the numerical simulation with a time step of  $\Delta t = 5.0 \cdot 10^{-7}$  s results in a steady-state value below 0.4 for the DC60 distortion parameter. Amplitudes of the dynamic data do not reach the peaks covered by the longer physical time steps. Whereas the number of iterations for the longer time steps seem to be sufficient to describe the steady-state and dynamic patterns of the DC60, more iterations are necessary for the shorter time step in order to gain valid data for the assessment of the distortion parameter. A comparison of flow field data for the three different time steps is

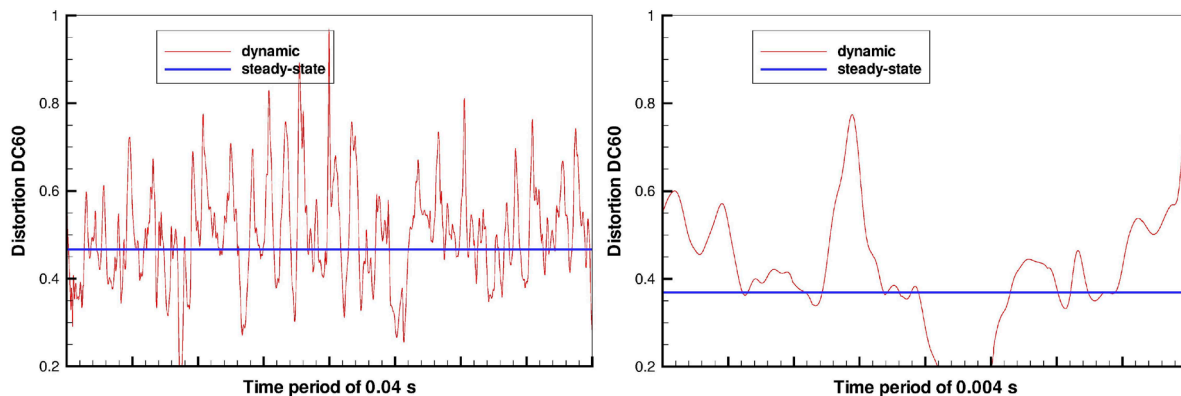


**Figure 15: Distortion parameter DC60 for steady state and dynamic simulations of the intake flow (section 3, engine face) for physical time steps of  $\Delta t = 5.0 \cdot 10^{-6}$  s (left) and  $\Delta t = 5.0 \cdot 10^{-7}$  s (right).**

provided in Fig. 16 displayed by Schlieren-like visualizations (magnitude of the density gradient). In general the resolved shear layer remains rather stable downstream of the flow separation at the S-bend of the lower duct wall and, proceeding, resulting in a strong distorted flow separation pattern. The turbulence of the shear layer in the instantaneous case is clearly illustrated and large eddies downstream of the bursting are obvious. The delay in the development of the instabilities in the shear layer can clearly be depicted from the Schlieren-like visualizations. On the top wall of the M2129 S-duct with extended length<sup>22</sup> separation also occurs but is not as pronounced as on the bottom wall.

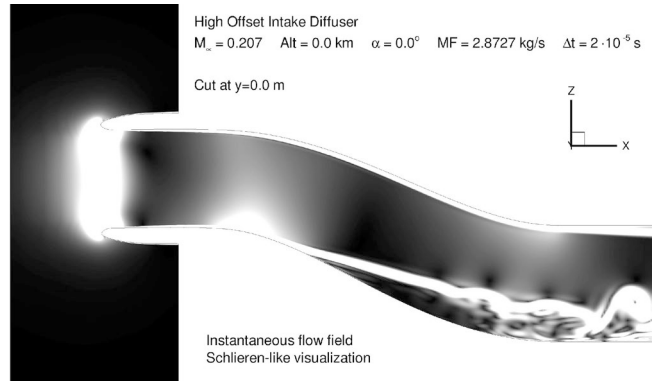
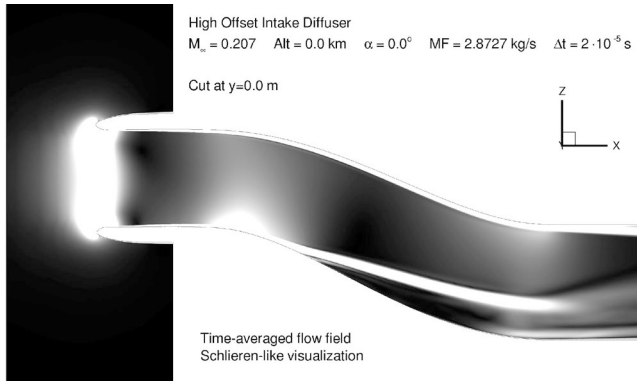
For shorter time steps the time-averaged solution for the shear layer and the separated flow becomes less distinct. Since the simulations at these time steps were run for an overall time period of 0.04 s and 0.004 s, respectively, more iterations would be necessary in order to improve the averaged results. The instantaneous data do not show major discrepancies. Further investigations and comparisons are mandatory in order to study these effects intensely and to find solutions for determining appropriate duration lengths for physical time steps. It would also be interesting to assess a grid refinement in the vicinity of the shear layer in order to avoid a delay in the development of the instabilities in the shear layer.

The results of the present DES computations are also documented in the GARTEUR Aerodynamics Action Group AD/AG-43 final report.<sup>21</sup>

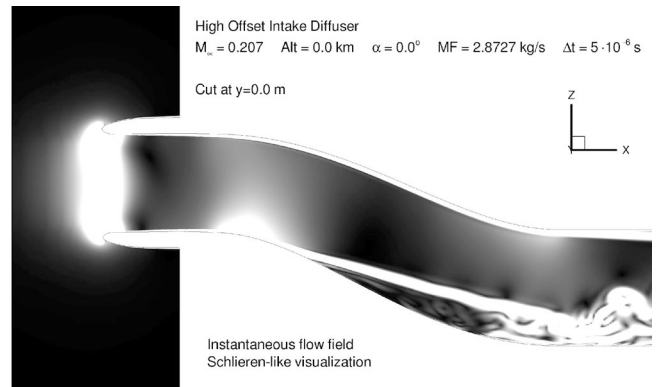
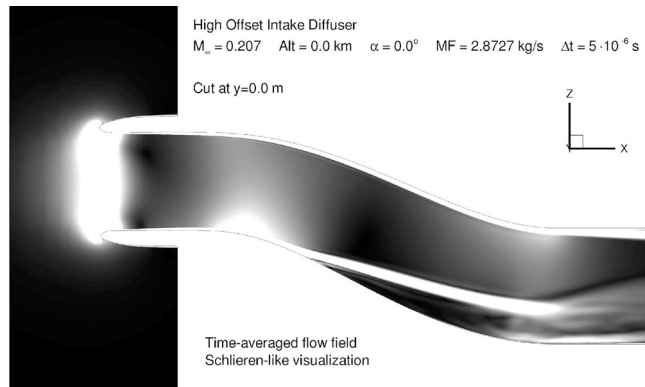
**Time-averaged**

**Instantaneous**

$\Delta t = 2.0 \cdot 10^{-5} \text{ s}$



$\Delta t = 5.0 \cdot 10^{-6} \text{ s}$



$\Delta t = 5.0 \cdot 10^{-7} \text{ s}$

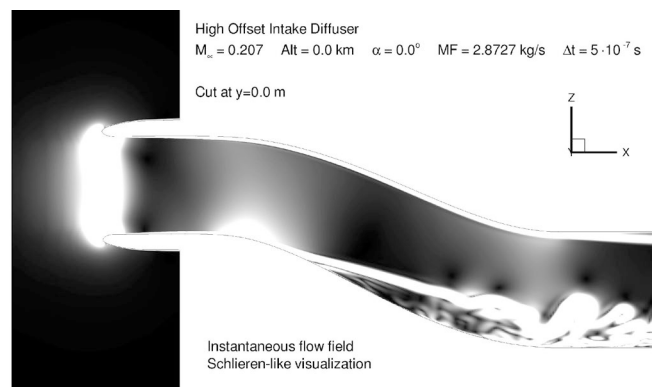
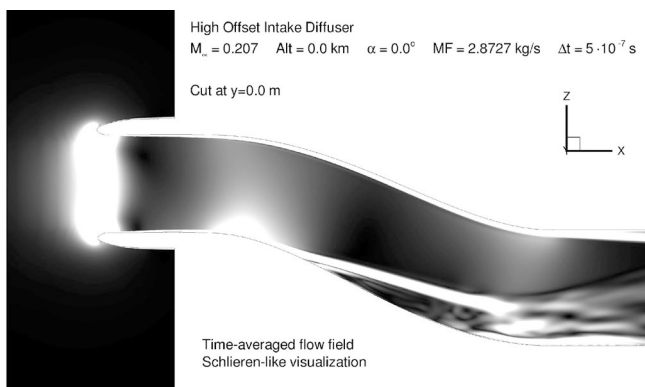


**Figure 16: Comparison of diffuser flow solutions (time-averaged and instantaneous flow field, Schlieren-like visualization) with different physical time steps applied.**

Time-averaged and instantaneous static pressure distributions along the walls of the diffuser are shown in Fig. 17 (port = upper wall, stbd = lower wall, top/bottom = side walls) with low pressure regions where the flow is expanded, e.g. at the lower wall. Unsteady peak fluctuations of the pressure distribution at the lower wall can be identified for the instantaneous case. The pressure distribution for the upper wall is not affected by time-dependent fluctuations in the diffuser flow field. While the pressure distributions on the side walls are identical for the time-averaged case, minor differences can be detected downstream of the separation at the lower wall for the instantaneous simulation.

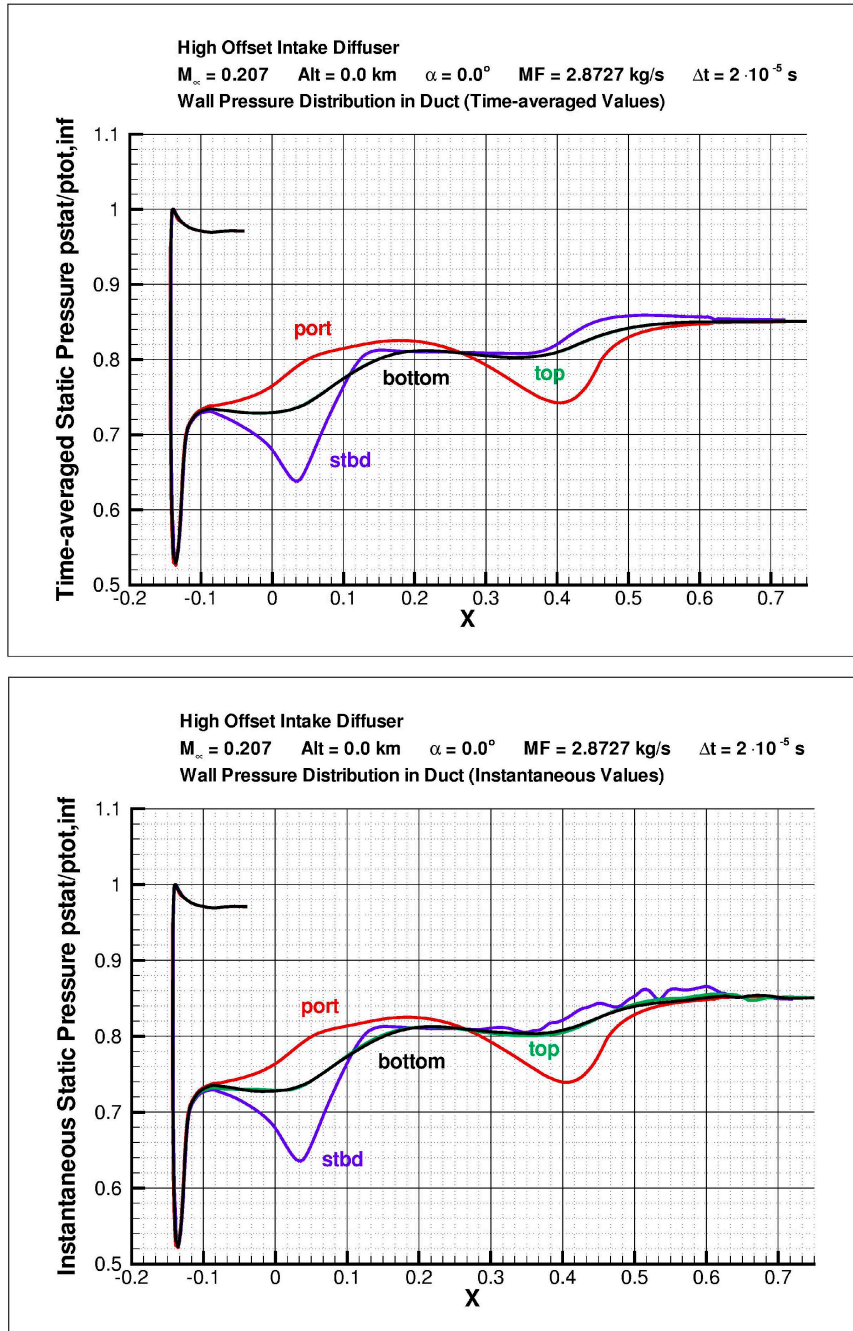


**Figure 17: Time-averaged and instantaneous static pressure distributions along the walls of the M2129 diffuser.**

## 5 Conclusion

Highly integrated air intakes with S-shaped diffusers have been investigated intensively in previous years since their application for advanced unmanned aerial vehicles will become more important in the future. Due to dissemination restrictions, however, only few investigations have been published, e.g. Ref. 1 and Ref. 23. To accompany the design process of such intake configurations, efficient hybrid CFD methods are a vital means of simulating the complex flow fields and reducing development time and cost. Hence there is a pressing need to evaluate the performance of such methods for this application.

The objective of the GARTEUR (Group for Aeronautical Research and Technology in EURope) Aerodynamics Action Group AD/AG-43 "Application of CFD to High Offset Intake Diffusers", consisting of EADS CASSIDIAN, ONERA, FOI, NLR, and QinetiQ, was the evaluation and demonstration of the capabilities and limitations of RANS, URANS, and especially DES methods in modeling the flow physics and performance characteristics of a compact high offset subsonic intake diffuser featuring a large separated flow region very difficult to accurately predict by CFD. These investigations were done by solving the full three-dimensional Navier-Stokes equations coupled with various turbulence models and by comparing the numerical results with experimental data from RAE (a predecessor of QinetiQ) M2129 wind tunnel tests.

Calculations were carried out for a specified test case having an onset flow Mach number of 0.207 for which experimental data were available. Computational results were compared with wind tunnel test data.

In RANS and time-averaged DES results, the global flow features are generally correctly captured, and the loss of total pressure as well as the Mach number are in good agreement with the experimental data at the engine face. The pattern of the region with total pressure losses for the numerical case has limited conformity with the experimental results. The DC60 distortion parameter, which is extremely sensitive to the local flow characteristics, is systematically overestimated, the deviation from the experimental value being higher for the DES solution than for the RANS result due to an overestimation of the separated flow region. DES results show a delay in the development of the instabilities in the shear layer. The fluctuations of the air inlet performance are induced by the dynamics of the reattachment process. Instantaneous Schlieren-like visualizations illustrate the roll-up of two-dimensional eddies created in the shear layer and their convection towards the engine entry face, while smaller three-dimensional structures are carried back towards the separated area, leading to a feedback mechanism.

The degree of unsteadiness of the solution obtained for the present test case with separated and reattached flow physics demonstrates that it is important to solve the large-scale time-dependent features of the flow. Recorded total pressure fluctuations require further analysis with respect to resonance frequencies, which might be harmful to compressor blades. The evaluation of the distortion parameter DC60 for steady state and dynamic simulations of the intake flow at the engine face revealed that distortion based on time-averaged or by steady numerical methods (e.g. RANS) generated values for the total pressures can actually not be used for the assessment of the engine/intake compatibility, since these values do not reflect the strong dynamic behavior of the flow in a high offset intake diffuser and would not lead to a correct assessment of the performance parameters considering the distortion limits required by the engine manufacturers.

Further needs for investigations and appropriate use of DES became obvious, including the assessment of the grid resolution in the free shear layer and the physical time step size on the computational results and hence the evaluation of the instantaneous DC60 distortion parameter. Since the finalization of GARTEUR AD/AG-43, further code improvements have been performed, especially dedicated to solving the delay in the formation of instabilities in the evolution of the shear layer.<sup>26</sup>

The present investigation also indicates that the prediction of time-variant total pressure distortion is possible using this approach, even if DES capabilities still need to be enhanced in order to reach accuracy levels that are required for industrial applications. In this respect, mid-term prospects of evaluating dynamic intake distortion parameters and of predicting engine/intake compatibility with numerical results for the total pressure distributions from DES calculations are deemed to be most promising. An additional payoff is an improved understanding of the flow physics in this class of diffuser, which in the future could lead to improvements in

diffuser flow handling and flow control systems. Current shortcomings relating to accuracy, computing time, computer memory capacity, data gathering and postprocessing efforts will certainly be overcome in the near future, and project-oriented applications will be made feasible. Improved prediction capabilities will have a positive impact on the ability to design such intake configurations efficiently and to reduce wind tunnel costs. In application, e.g. to UAVs, this would mean the ability to improve the combined relationship among vital design factors such as observability, weight, range, and manufacturing costs. The work performed in GARTEUR AD/AG-43 has been continued in AD/AG-46 "Highly Integrated Subsonic Air Intakes" with application of improved DES methods to a complete UAV configuration.<sup>24-29</sup>

## Acknowledgments

The authors would like to express their thanks to Phil Tattersall (formerly QinetiQ) for the provision of the experimental data from RAE M2129 wind tunnel tests. The contribution of Roald Waaijer with his Master's Thesis to the NLR investigations is greatly appreciated.

## References

- <sup>1</sup>Mace, J., Lakebrink, M., Mani, M., and Steenken, W., "Computational Simulation of Dynamic Total-Pressure Distortion in an S-Diffuser," AIAA Paper 2012-3999, August 2012.
- <sup>2</sup>Delot, A.-L. and Scharnhorst, R. K., "A Comparison of Several CFD Codes with Experimental Data in a Diffusing S-Duct," AIAA-2013-3796, *49th AIAA/ASME/SAE/ASEE Joint Propulsion Conference*, 14-17 July 2013, San Jose, CA, USA, with results of the first AIAA "Propulsion Aerodynamics Workshop," sponsored by the Air Breathing Propulsion System Integration Technical Committee, held on July 29, 2012 at the 48th AIAA Joint Propulsion Conference in Atlanta, Georgia.
- <sup>3</sup>Strelets, M., "Detached Eddy Simulation of Massively Separated Flows," AIAA-2001-0879.
- <sup>4</sup>Spalart, P.R., "Topics in Detached Eddy Simulation," ICCFD3, Toronto, Canada, July 2004.
- <sup>5</sup>Deck, S., "Zonal-Detached-Eddy Simulation of the Flow Around a High-Lift Configuration," *AIAA Journal*, 43(11) : 2372–2384, November 2005.
- <sup>6</sup>Vuillerme, A.-L., Deck, S., and Chevrier, R., "Numerical Simulations of the Flow Inside an S-shaped Intake Diffuser," *European Conference for Aerospace Sciences (EUCASS)*, Session 2.4 "CFD Simulation I", Moscow, Russia, 4-7 July 2005.
- <sup>7</sup>Menter, F., Kuntz, M., and Bender, R., "A Scale-Adaptive Simulation Model for Turbulent Flow Predictions," AIAA-2003-767
- <sup>8</sup>Consigny, H., Vasseur, O., and Delot, A.-L., "An Overview of the Group for Aeronautical Research and Technology in EUROPE (GARTEUR)," *AIAA Science and Technology Forum and Exposition*, 13-17 January 2014, National Harbor, MD, USA (submitted for publication).
- <sup>9</sup>Eliasson, P., "EDGE, a Navier–Stokes Solver for Unstructured Grids," Computational Aerodynamics Department, Aeronautics Division, FOI, Stockholm, 2001.
- <sup>10</sup>Spalart, P. R., Jou, W. H., Strelets, M., & Allmaras, S. R., "Comments on the Feasibility of LES for Wings, and on a Hybrid RANS/LES Approach," in C. Liu, & Z. Liu (Ed.), *1st AFOSR Int. Conf. on DNS/LES, Advances in DNS/LES* (pp. 137-148), Ruston: Greyden Press, 1997.
- <sup>11</sup>Peng, S.-H., "Algebraic Hybrid RANS-LES Modeling Applied to Incompressible and Unsteady RANS," AIAA Paper, 3910, 2006.
- <sup>12</sup>Spalart P.R., Allmaras S.R., "A One-Equation Turbulence Model for Aerodynamic Flows," *Proceedings of the 30th AIAA Aerospace Sciences Meeting and Exhibit*, AIAA 1992-0439, Reno, Nevada, 1992.
- <sup>13</sup>Wallin, S. and Johansson, A., "An Explicit Algebraic Reynolds Stress Model for Incompressible and Compressible Turbulent Flows," *Journal of Fluid Mechanics*, 89-132, 2000.
- <sup>14</sup>Nikitin, N. V., Nicoud, F., Wasistho, B., Squires, K. D., and Spalart, P. R., "An Approach to Wall Modeling in Large Eddy Simulation," *Physics of Fluids*, 12, 1629-1632, 2000.

<sup>15</sup>Spalart, P. R., Deck, S., Shur, M. L., Squires, K. D., Strelets, M. K., and Travin, A., "A New Version of Detached-Eddy Simulation, Resistant to Ambiguous Grid Densities," *Theoretical and Computational Fluid Dynamics*, 20, 181-195, 2006.

<sup>16</sup>Deck, S., "Zonal-Detached-Eddy Simulation of the Flow Around a High-Lift Configuration," *AIAA Journal*, 43 (11), 2372-2384, November 2005.

<sup>17</sup>Boerstoel, J. W., Kassies, A., Kok, J. C., and Spekrijse, S. P., "ENFLOW, a Full-Functionality System of CFD Codes for Industrial Euler/Navier-Stokes Flow Computations," National Aerospace Laboratory NLR, NLR-TP-96286, 1996.

<sup>18</sup>Kok, J. C., "Efficient and Accurate Implementation of the k-omega Turbulence Model in the NLR Multi-Block Navier-Stokes System," National Aerospace Laboratory NLR, NLR-TP-2000-144, 2000.

<sup>19</sup>Waaiker, R. A., "Separated Flows in Highly Offset Inlets," Master's Thesis, National Aerospace Laboratory, NLR Report NLR-TR-2007-349, June 2007.

<sup>20</sup>Schwamborn, D., Gerhold, T., and Kessler, K., "DLR-TAU Code – an Overview," *Proceedings of the 1st ONERA/DLR Aerospace Symposium*, Paris, France, 1999.

<sup>21</sup>Berens, T. M., Delot, A.-L., Chevalier, M., Van Muijden, J., Waaiker, R. A., and Tattersall, P., "Application of CFD to High Offset Intake Diffusers," Group for Aeronautical Research and Technology in EUROpe (GARTEUR), AD/AG-43 Final Report, GARTEUR TP-173, October 2012, to be published on GARTEUR Website <http://www.garteur.eu>.

<sup>22</sup>Chevalier, M., & Peng, S.-H., "Detached Eddy Simulation of Turbulent Flow in a Highly Offset Intake Diffuser," in S.-H. Peng & W. Haase (Ed.), *2007 Symposium of Hybrid RANS-LES Methods* (pp. 111-121), Springer-Verlag Berlin Heidelberg, 2010.

<sup>23</sup>Vuillerme, A., Deck, S., & Chevrier, R., "Numerical Simulations of the Flow Inside an S-shaped Intake Diffuser," European Conference for Aerospace Sciences (EUCASS), Moscow, 2005.

<sup>24</sup>Berens, T. M., Delot, A.-L., Tormalm, M. H., Ruiz-Calavera, L.-P., Funes-Sebastian, D.-E., Rein, M., Säterskog, M., Ceresola, N., and Zurawski, L., "Numerical and Experimental Investigations on Highly Integrated Subsonic Air Intakes," *AIAA Science and Technology Forum and Exposition*, 13-17 January 2014, National Harbor, MD, USA (submitted for publication).

<sup>25</sup>Delot, A.-L., Berens, T. M., Tormalm, M. H., Säterskog, M., and Ceresola, N., "DES Computations for a Subsonic UAV Configuration with a Highly Integrated S-Shaped Intake Duct," *AIAA Science and Technology Forum and Exposition*, 13-17 January 2014, National Harbor, MD, USA (submitted for publication).

<sup>26</sup>Tormalm, M. H., "Flow Control Using Vortex Generators or Micro-Jets Applied in a UCAV Intake," *AIAA Science and Technology Forum and Exposition*, 13-17 January 2014, National Harbor, MD, USA (submitted for publication).

<sup>27</sup>Funes-Sebastian, D.-E. and Ruiz-Calavera, L.-P., "Numerical Simulations of Wind Tunnel Effects on Intake Flow of a UAV Configuration," *AIAA Science and Technology Forum and Exposition*, 13-17 January 2014, National Harbor, MD, USA (submitted for publication).

<sup>28</sup>Rein, M., Koch, S., and Ruetten, M., "Experimental and Numerical Investigations on the Influence of Ingesting Boundary Layers into a Diverterless S-Duct Intake," *AIAA Science and Technology Forum and Exposition*, 13-17 January 2014, National Harbor, MD, USA (submitted for publication).

<sup>29</sup>Berens, T. M., Delot, A.-L., Tormalm, M. H., Ruiz-Calavera, L.-P., Funes-Sebastian, D.-E., Rein, M., Säterskog, M., Ceresola, N., and Zurawski, L., "Highly Integrated Subsonic Air Intakes," Group for Aeronautical Research and Technology in EUROpe (GARTEUR), AD/AG-46 Final Report, to be published on GARTEUR Website <http://www.garteur.eu> in 2014.